Modal Analysis of All-Walls Longitudinally Corrugated Rectangular Waveguides Using Asymptotic Corrugations Boundary Conditions

Malcolm Ng Mou Kehn, *Senior Member, IEEE*

***Abstract*—The asymptotic corrugations boundary conditions (ACBCs) are used together with classical theory of vector potentials and an innovative combination of matrix systems to analyze rectangular waveguides having all four walls being longitudinally (axially) corrugated. One matrix system is composed of the ACBCs of two opposite walls, while the other comprises those of the other pair of corrugated walls. A transcendental characteristic equation is derived, from which the modal dispersion diagram can be obtained, for all three modal wave-tyoes: fast space, slow surface, and evanescent waves. From the formulation, analytical modal field functions in closed form are also acquired. Results of dispersion graphs and modal field distributions generated by this method are compared favorably with those obtained by a commercial full-wave solver.**

***Index Terms*—Asymptotic corrugations boundary condition (ACBC), corrugated waveguides, dispersion diagram.**

I. Introduction

THE corrugated waveguide has been a useful device for microwave and antenna applications. Transversely corrugated waveguides or horns, known also as hybrid-mode horns or soft horns, are commonly engaged as the primary feeds for reflectors [1]–[3] due to their low cross polarization and low sidelobes. However, longitudinally corrugated ones find applications as cluster feeds of reflector antennas due to their high aperture efficiencies [4]. Quasi-TEM modes with near uniform aperture field distribution supported by such axially grated hard-walled waveguides have also been proposed as effective elements in multifunction interlaced arrays [5] and vital components in quasi-optical grid amplifiers [6]. Other applications of hard corrugated waveguides include mode converters [7], [8], polarization transformers [9], as well as resonant cavities [10].

As far as what could be found in the literature, prior works on corrugated waveguides may be grouped into the following categories: 1) circular waveguides that are either a) transversely [10]–[18] or b) longitudinally [9] corrugated and 2) rectangular waveguides having either a) just two opposite walls that are i) transversely [19] or ii) longitudinally [20] corrugated or b) only one out of the four walls that is transversely corrugated [21], [22]. Despite all of the extensive literature, none has attempted to analyze the rectangular waveguide with all four walls being longitudinally corrugated, with the possible exception of the valiant efforts by Pierre *et al.* [23]. The corrugated circular waveguide has a simpler geometry to treat because there is only one other independent coordinate variable (specifically, the azimuth phi) in addition to the axial z that is tangential to the entire (smooth circular) interface separating the central portion from the concentric corrugated region. On the contrary, the rectangular waveguide with all its walls corrugated has four separate smooth (flat) interfaces involving both transverse coordinate variables (x and y). As a result, it is not possible to construct a solvable system of equations and thus obtain modal solutions merely by classical analysis methods just in their conventional forms. As the literature survey has indeed shown, considerably more investigations of the circular rather than the rectangular geometry have been reported, with stronger attention on transverse rather than longitudinal corrugations being also apparent.

A recent work has presented in detail the use of the asymptotic corrugations boundary conditions (ACBCs) for obtaining the modal surface-wave field solutions and dispersive propagation properties of open planar corrugated surfaces [24]. This paper proposes a novel way to solve the all-four-walls axially corrugated rectangular waveguide by amalgamating the traditional vector potential modal analysis with the ACBC, but not without the innovation of considering two linear systems of equations: one pertaining to the ACBCs of the left and right corrugated walls, while the other associated with those of the upper and lower corrugated walls, and then combining them. An analytical closed-form transcendental characteristic equation is then acquired. Modal field functions are also obtained as closed-form mathematical expressions for all modal wavetypes: fast propagating modal space waves, slow modal surface waves, and evanescent modes. Results of dispersion diagrams and modal field distributions computed according to the proposed theory will be compared with those generated by the commercial full-wave solver CST Microwave Studio.

II. Theory and Formulation

Consider the longitudinally corrugated rectangular waveguide of Fig. 1. The width and height along x and y of the central region with medium parameters ($\varepsilon_{\rm cen}$ & $\mu_{\rm cen}$) are $2a$ and $2b$, respectively. The depth of the corrugations on both side waveguide walls is d, whereas that of the upper and lower walls is c. The common period (unit cell size) along x of the corrugations on the upper and lower walls is p_x, whereas that along y on the left and right walls is p_y. For simplicity of

Manuscript received May 20, 2013; revised September 05, 2013; accepted September 06, 2013. Date of publication October 07, 2013; date of current version November 01, 2013. This work was supported by the National Science Council of Taiwan.

The author is with the Department of Electrical Engineering, National Chiao Tung University (NCTU), Hsinchu 30010, Taiwan (e-mail: malcolm.ng@ieee.org).

Color versions of one or more of the figures in this paper are available online at http://ieeexplore.ieee.org.

Digital Object Identifier 10.1109/TMTT.2013.2283843

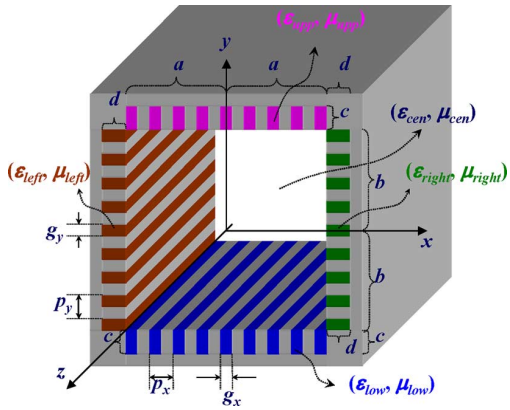

Fig. 1. Longitudinally corrugated rectangular waveguide.

the formulation, although not necessary, the gratings on all four walls share a common groove width g_w to period p_w ratio, g_w/p_w, where w may be x or y. The associated metallic ridge thickness is then $t_w = p_w - g_w$. The generally different permittivities and permeabilities of the four media filling the grooves of the various corrugated walls are $(\varepsilon_{\rm left}\,\&\,\mu_{\rm left})$, $(\varepsilon_{\rm right}\,\&\,\mu_{\rm right})$, $(\varepsilon_{\rm upp}\,\&\,\mu_{\rm upp})$, and $(\varepsilon_{\rm low}\,\&\,\mu_{\rm low})$, in which the subscripts denote the gratings on the left, right, upper, and lower walls.

A. Modal Fields by Vector Potentials

1) Within Grooves of Corrugations: The fields within the corrugation grooves are derived by classical vector potential analyses [25] *for modes that are TE and TM to the direction perpendicular to each respective corrugated surface*, and the enforcement of appropriate boundary conditions requiring the vanishing of tangential electric field components on the metallic walls of the grooves. Doing so, the x, y, and z components of the E and H fields of the TE and TM modal fields within the various grooves are stated as follow; these upcoming expressions are also more directly derived in [20]–[24].

a) Left Groove: $-(a+d) < x < -a$; $-g_y/2 < y < g_y/2$ *and Right Groove:* $a < x < a+d$; $-g_y/2 < y < g_y/2$ *(TE and TM to x):*

$$\begin{bmatrix} \overset{\rm side}{E}{}^{\rm TE}_{y(n^{\rm side}_{\rm TE})} \\ \overset{\rm side}{H}{}^{\rm TM}_{y(n^{\rm side}_{\rm TM})} \end{bmatrix} = jk_z^{\rm univ} \begin{bmatrix} \overset{\rm side}{\zeta}{}^{\rm TE}_{x_{\rm sin}} \overset{\rm side}{\zeta}{}^{\rm TE}_{y_{\rm cos}} S^{\rm side}_{x_{\rm TE}} C^{\rm side}_{y_{\rm TE}} \Big/ \varepsilon_{\rm side} \\ -\overset{\rm side}{\zeta}{}^{\rm TM}_{x_{\rm cos}} \overset{\rm side}{\zeta}{}^{\rm TM}_{y_{\rm sin}} C^{\rm side}_{x_{\rm TM}} S^{\rm side}_{y_{\rm TM}} \Big/ \mu_{\rm side} \end{bmatrix} \tag{1a}$$

$$\begin{bmatrix} \overset{\rm side}{E}{}^{\rm TE}_{z(n^{\rm side}_{\rm TE})} \\ \overset{\rm side}{H}{}^{\rm TM}_{z(n^{\rm side}_{\rm TM})} \end{bmatrix} = - \begin{bmatrix} k^{\rm side}_{y_{\rm TE}} \overset{\rm side}{\zeta}{}^{\rm TE}_{x_{\rm sin}} \overset{\rm side}{\zeta}{}^{\rm TE}_{y_{\rm cos}} S^{\rm side}_{x_{\rm TE}} S^{\rm side}_{y_{\rm TE}} \Big/ \varepsilon_{\rm side} \\ k^{\rm side}_{y_{\rm TM}} \overset{\rm side}{\zeta}{}^{\rm TM}_{x_{\rm cos}} \overset{\rm side}{\zeta}{}^{\rm TM}_{y_{\rm sin}} C^{\rm side}_{x_{\rm TM}} C^{\rm side}_{y_{\rm TM}} \Big/ \mu_{\rm side} \end{bmatrix} \tag{1b}$$

$$\begin{bmatrix} \overset{\rm side}{H}{}^{\rm TE}_{x(n^{\rm side}_{\rm TE})} \\ \overset{\rm side}{E}{}^{\rm TM}_{x(n^{\rm side}_{\rm TM})} \end{bmatrix} = \frac{k^2_{\rm side} - \begin{bmatrix} \left(k^{\rm side}_{x_{\rm TE}}\right)^2 \\ \left(k^{\rm side}_{x_{\rm TM}}\right)^2 \end{bmatrix}}{j\omega\mu_{\rm side}\varepsilon_{\rm side}} \times \begin{bmatrix} \overset{\rm side}{\zeta}{}^{\rm TE}_{x_{\rm sin}} \overset{\rm side}{\zeta}{}^{\rm TE}_{y_{\rm cos}} S^{\rm side}_{x_{\rm TE}} C^{\rm side}_{y_{\rm TE}} \\ \overset{\rm side}{\zeta}{}^{\rm TM}_{x_{\rm cos}} \overset{\rm side}{\zeta}{}^{\rm TM}_{y_{\rm sin}} C^{\rm side}_{x_{\rm TM}} S^{\rm side}_{y_{\rm TM}} \end{bmatrix} \tag{1c}$$

$$\begin{bmatrix} \overset{\rm side}{H}{}^{\rm TE}_{y(n^{\rm side}_{\rm TE})} \\ \overset{\rm side}{E}{}^{\rm TM}_{y(n^{\rm side}_{\rm TM})} \end{bmatrix} = -\frac{1}{j\omega\mu_{\rm side}\varepsilon_{\rm side}} \times \begin{Bmatrix} k^{\rm side}_{x_{\rm TE}} k^{\rm side}_{y_{\rm TE}} \overset{\rm side}{\zeta}{}^{\rm TE}_{x_{\rm sin}} \overset{\rm side}{\zeta}{}^{\rm TE}_{y_{\rm cos}} C^{\rm side}_{x_{\rm TE}} S^{\rm side}_{y_{\rm TE}} \\ k^{\rm side}_{x_{\rm TM}} k^{\rm side}_{y_{\rm TM}} \overset{\rm side}{\zeta}{}^{\rm TM}_{x_{\rm cos}} \overset{\rm side}{\zeta}{}^{\rm TM}_{y_{\rm sin}} S^{\rm side}_{x_{\rm TM}} C^{\rm side}_{y_{\rm TM}} \end{Bmatrix} \tag{1d}$$

$$\begin{bmatrix} \overset{\rm side}{H}{}^{\rm TE}_{z(n^{\rm side}_{\rm TE})} \\ \overset{\rm side}{E}{}^{\rm TM}_{z(n^{\rm side}_{\rm TM})} \end{bmatrix} = \frac{jk_z^{\rm univ}}{j\omega\mu_{\rm side}\varepsilon_{\rm side}} \times \begin{bmatrix} -k^{\rm side}_{x_{\rm TE}} \overset{\rm side}{\zeta}{}^{\rm TE}_{x_{\rm sin}} \overset{\rm side}{\zeta}{}^{\rm TE}_{y_{\rm cos}} C^{\rm side}_{x_{\rm TE}} C^{\rm side}_{y_{\rm TE}} \\ k^{\rm side}_{x_{\rm TM}} \overset{\rm side}{\zeta}{}^{\rm TM}_{x_{\rm cos}} \overset{\rm side}{\zeta}{}^{\rm TM}_{y_{\rm sin}} S^{\rm side}_{x_{\rm TM}} S^{\rm side}_{y_{\rm TM}} \end{bmatrix} \tag{1e}$$

$$\overset{\rm side}{E}{}^{\rm TE}_{x} = 0 \quad \overset{\rm side}{H}{}^{\rm TM}_{x} = 0 \tag{1f}$$

$$S^{\{\overset{\rm left}{\rm right}\}}_{x_{T\psi}} = \sin\left[k^{\{\overset{\rm left}{\rm right}\}}_{x_{T\psi}}(x \pm a \pm d)\right], \quad \psi = E \text{ or } M \tag{1gi}$$

$$C^{\{\overset{\rm left}{\rm right}\}}_{x_{T\psi}} = \cos\left[k^{\{\overset{\rm left}{\rm right}\}}_{x_{T\psi}}(x \pm a \pm d)\right], \quad \psi = E \text{ or } M \tag{1gii}$$

$$S^{\rm side}_{y_{T\psi}} = \sin\left[k^{\rm side}_{y_{T\psi}}\left(y + \frac{g_y}{2}\right)\right]$$

$$C^{\rm side}_{y_{T\psi}} = \cos\left[k^{\rm side}_{y_{T\psi}}\left(y + \frac{g_y}{2}\right)\right] \tag{1h}$$

$$k^{\rm side}_{y_{T\psi}} = n^{\rm side}_{T\psi}\pi/g_y \quad n^{\rm side}_{T\psi} = \text{integer} \tag{1i}$$

$$k_{\rm side} = \omega\sqrt{\mu_{\rm side}\varepsilon_{\rm side}} = \sqrt{\left(k^{\rm side}_{x_{T\psi}}\right)^2 + \left(k^{\rm side}_{y_{T\psi}}\right)^2 + \left(k_z^{\rm univ}\right)^2} \tag{1j}$$

whereby the scripts "side" may denote either "*left*" or "*right*." In (1gi) and (1gii), the left and right within the superscripted curly braces pertain to the $+$ and $-$ signs of the $\pm$ in $(x \pm a \pm d)$, respectively. The $\overset{\rm side}{\zeta}{}^{T\psi}_{w_\tau}$, in which ψ is E or M, w is x or y, and τ is "sin" or "cos" represents an amplitude coefficient, with its w subscript merely indicative of the coordinate argument of the sine or cosine (represented by τ) functional variation of the original vector potentials. The ψ of $T\psi$ in (1gi) and (1gii) may be E or M. The $k^{\rm side}_{w_{T\psi}}$ for $w = x$ or y is the usual wavenumber component along that associated direction, whereas the superscript univ of $k_z^{\rm univ}$ signifies the universality of the propagation constant along the axial z direction that is shared by all regions of the waveguide due to phase continuity. The integer $n^{\rm side}_{T\psi}$ symbolizes the modal index representing the number of half-cycle field variations along y within the groove, being the direction perpendicular to the gratings. Lastly, of course, the TE and TM scripts label the two modal groups. The symbols C and S of (1g) and (1h) are introduced to abbreviate the notation. Note that in all these above field expressions, a multiplicative term $\exp(-jk_z^{\rm univ}z)$ has been assumed and suppressed.

b) Upper Groove: $-g_x/2 < x < g_x/2$; $b < y < b+c$ *and Lower Groove:* $-g_x/2 < x < g_x/2$; $-b-c < y < -b$ *(TE and TM to y):* The field components in the upper and lower groove regions may be obtained by performing the following changes to (1a)–(1j).

i) Change all "side" scripts to "u and ℓ."

ii) To the right-hand sides of (1a)–(1j), except (1f) and (1i), which contain neither x, nor y, interchange all x and y, i.e., all x become y and vice-versa.

iii) To all field symbols of (1a)–(1f), except (1b) and (1e) for the z-components, likewise interchange all x and y subscripts.
iv) Negate the expressions transformed from (1a) and (1b).
v) For (1gi) and (1gii), change the "left," "right," a, d, and $\pm$ to "upp," "low," b, c, and $\mp$, respectively.
vi) Change all y subscripts in (1i) to x.

In these transformed expressions, the scripts "u and ℓ" may denote either "upp" or "low." All new symbols, scripts, and notations that arise bear the same corresponding descriptions as those in (1a)–(1j). As before, a multiplicative term $\exp(-jk_z^{\text{univ}} z)$ has been assumed and suppressed in all field terms.

2) Modal TE^x *and* TM^x *Fields Within Central Region:* $-a < x < a$; $-b < y < b$ *(TE and TM to* x *Only):* By vector potential analysis as well, the various components of the E and H fields of the modal fields in the central region of the waveguide may be written. This time, however, modes that are TE and TM to just one of the two transverse directions (x and y) are considered, being chosen arbitrarily to be the horizontal x coordinate in the present formulation. The same efficacy of the analysis is maintained if y is used instead.

a) TE^x *Mode:*

$$E_x^{\text{cen}\,\text{TE}^x} = 0 \tag{2ai}$$

$$E_y^{\text{cen}\,\text{TE}^x} = \frac{jk_z^{\text{univ}}}{\varepsilon_{\text{cen}}} \begin{bmatrix} \left(\zeta_{x_{\cos}}^{\text{cen}\,\text{TE}^x} C_{x_{\text{TE}}}^{\text{cen}} + \zeta_{x_{\sin}}^{\text{cen}\,\text{TE}^x} S_{x_{\text{TE}}}^{\text{cen}}\right) \times \\ \left(\zeta_{y_{\cos}}^{\text{cen}\,\text{TE}^x} C_{y_{\text{TE}}}^{\text{cen}} + \zeta_{y_{\sin}}^{\text{cen}\,\text{TE}^x} S_{y_{\text{TE}}}^{\text{cen}}\right) \end{bmatrix} \tag{2aii}$$

$$E_z^{\text{cen}\,\text{TE}^x} = \frac{k_{y_{\text{TE}^x}}^{\text{cen}}}{\varepsilon_{\text{cen}}} \begin{bmatrix} \left(\zeta_{x_{\cos}}^{\text{cen}\,\text{TE}^x} C_{x_{\text{TE}}}^{\text{cen}} + \zeta_{x_{\sin}}^{\text{cen}\,\text{TE}^x} S_{x_{\text{TE}}}^{\text{cen}}\right) \times \\ \left(\zeta_{y_{\sin}}^{\text{cen}\,\text{TE}^x} C_{y_{\text{TE}}}^{\text{cen}} - \zeta_{y_{\cos}}^{\text{cen}\,\text{TE}^x} S_{y_{\text{TE}}}^{\text{cen}}\right) \end{bmatrix} \tag{2aiii}$$

$$H_x^{\text{cen}\,\text{TE}^x} = \frac{k_{\text{cen}}^2 - \left(k_{x_{\text{TE}^x}}^{\text{cen}}\right)^2}{j\omega\mu_{\text{cen}}\varepsilon_{\text{cen}}} \begin{bmatrix} \left(\zeta_{x_{\cos}}^{\text{cen}\,\text{TE}^x} C_{x_{\text{TE}}}^{\text{cen}} + \zeta_{x_{\sin}}^{\text{cen}\,\text{TE}^x} S_{x_{\text{TE}}}^{\text{cen}}\right) \times \\ \left(\zeta_{y_{\cos}}^{\text{cen}\,\text{TE}^x} C_{y_{\text{TE}}}^{\text{cen}} + \zeta_{y_{\sin}}^{\text{cen}\,\text{TE}^x} S_{y_{\text{TE}}}^{\text{cen}}\right) \end{bmatrix} \tag{2bi}$$

$$H_y^{\text{cen}\,\text{TE}^x} = \frac{k_{x_{\text{TE}^x}}^{\text{cen}} k_{y_{\text{TE}^x}}^{\text{cen}}}{j\omega\mu_{\text{cen}}\varepsilon_{\text{cen}}} \begin{bmatrix} \left(\zeta_{x_{\sin}}^{\text{cen}\,\text{TE}^x} C_{x_{\text{TE}}}^{\text{cen}} - \zeta_{x_{\cos}}^{\text{cen}\,\text{TE}^x} S_{x_{\text{TE}}}^{\text{cen}}\right) \times \\ \left(\zeta_{y_{\sin}}^{\text{cen}\,\text{TE}^x} C_{y_{\text{TE}}}^{\text{cen}} - \zeta_{y_{\cos}}^{\text{cen}\,\text{TE}^x} S_{y_{\text{TE}}}^{\text{cen}}\right) \end{bmatrix} \tag{2bii}$$

$$H_z^{\text{cen}\,\text{TE}^x} = \frac{k_z^{\text{univ}} k_{x_{\text{TE}^x}}^{\text{cen}}}{\omega\mu_{\text{cen}}\varepsilon_{\text{cen}}} \begin{bmatrix} \left(\zeta_{x_{\cos}}^{\text{cen}\,\text{TE}^x} S_{x_{\text{TE}}}^{\text{cen}} - \zeta_{x_{\sin}}^{\text{cen}\,\text{TE}^x} C_{x_{\text{TE}}}^{\text{cen}}\right) \times \\ \left(\zeta_{y_{\cos}}^{\text{cen}\,\text{TE}^x} C_{y_{\text{TE}}}^{\text{cen}} + \zeta_{y_{\sin}}^{\text{cen}\,\text{TE}^x} S_{y_{\text{TE}}}^{\text{cen}}\right) \end{bmatrix} \tag{2biii}$$

$$\begin{bmatrix} C_{w_{T\psi}}^{\text{cen}} \\ S_{w_{T\psi}}^{\text{cen}} \end{bmatrix} = \begin{bmatrix} \cos\left(k_{w_{T_\psi x}}^{\text{cen}} w\right) \\ \sin\left(k_{w_{T\psi^x}}^{\text{cen}} w\right) \end{bmatrix}, \quad \psi = E \text{ or } M; \quad w = x \text{ or } y \tag{2c}$$

$$k_{\text{cen}} = \omega\sqrt{\mu_{\text{cen}}\varepsilon_{\text{cen}}} = \sqrt{\left(k_{x_{T\psi^x}}^{\text{cen}}\right)^2 + \left(k_{y_{T\psi^x}}^{\text{cen}}\right)^2 + \left(k_z^{\text{univ}}\right)^2}. \tag{2d}$$

As was before for the groove fields, $\zeta_{w_\tau}^{T\psi^x}$ here, in which ψ is E or M, w is x or y, τ is "sin" or "cos" symbolizes an amplitude coefficient attached to the sine or cosine functional variation with x or y [as conveyed by (2c)] of the originating TE or TM vector potential function for the central region. Likewise, $k_{w_{T\psi^x}}^{\text{cen}}$ represents the wavenumber along x or y in the central region for the TE or TM mode. Of course, all scripts "cen" indicate that their associated quantities pertain to the central region.

b) TM^x *Mode:* The fields for the TM^x mode may be obtained by incorporating the following changes to the latter (2ai)–(2biii).

i) Change all TE to TM and all ε_{cen} to μ_{cen}.
ii) Interchange all E and H field symbols, i.e., E becomes H and vice-versa.
iii) Negate the expressions transformed from (2aii) and (2aiii), i.e., multiply their right-hand sides by -1.

Notice that the relations in (2c) and (2d) are already in forms that are applicable to both TE^x and TM^x modes.

B. ACBCs

Defining first the unit vector parallel and orthogonal to the corrugations as $\hat{a}_p$ and $\hat{a}_o$, respectively, the former being $\hat{z}$, while the latter being either $\hat{x}$ or $\hat{y}$ (unit vectors along z, x, or y) in the present context, the ACBCs enforced at the corrugated surface are stated as follows:

$$\vec{E}^{\text{grv}} \cdot \hat{a}_p = 0 \tag{3a}$$

$$\vec{E}^{\text{cen}} \cdot \hat{a}_p = 0 \tag{3b}$$

$$\vec{E}^{\text{grv}} \cdot \hat{a}_o = \vec{E}^{\text{cen}} \cdot \hat{a}_o \tag{3c}$$

$$\vec{H}^{\text{grv}} \cdot \hat{a}_p = \vec{H}^{\text{cen}} \cdot \hat{a}_p \tag{3d}$$

where

$$\vec{E}^{\text{grv}} = \sum_{n_{\text{TE}}^{\text{grv}}} \Big[\hat{x}(1-\delta_{\text{grv,side}}) E_{x(n_{\text{TE}}^{\text{grv}})}^{\text{grv}\,\text{TE}} + \hat{y}(1-\delta_{\text{grv},u\,\&\,\ell}) E_{y(n_{\text{TE}}^{\text{grv}})}^{\text{grv}\,\text{TE}} + \hat{z} E_{z(n_{\text{TE}}^{\text{grv}})}^{\text{grv}\,\text{TE}}\Big] + \sum_{n_{\text{TM}}^{\text{grv}}} \Big[\hat{x} E_{x(n_{\text{TM}}^{\text{grv}})}^{\text{grv}\,\text{TM}} + \hat{y} E_{y(n_{\text{TM}}^{\text{grv}})}^{\text{grv}\,\text{TM}} + \hat{z} E_{z(n_{\text{TM}}^{\text{grv}})}^{\text{grv}\,\text{TM}}\Big] \tag{4a}$$

$$\vec{H}^{\text{grv}} = \sum_{n_{\text{TE}}^{\text{grv}}} \Big[\hat{x} H_{x(n_{\text{TE}}^{\text{grv}})}^{\text{grv}\,\text{TM}} + \hat{y} H_{y(n_{\text{TE}}^{\text{grv}})}^{\text{grv}\,\text{TM}} + \hat{z} H_{z(n_{\text{TE}}^{\text{grv}})}^{\text{grv}\,\text{TM}}\Big] + \sum_{n_{\text{TM}}^{\text{grv}}} \Big[\hat{x}(1-\delta_{\text{grv,side}}) H_{x(n_{\text{TM}}^{\text{grv}})}^{\text{grv}\,\text{TE}} + \hat{y}(1-\delta_{\text{grv},u\,\&\,\ell}) H_{y(n_{\text{TM}}^{\text{grv}})}^{\text{grv}\,\text{TE}} + \hat{z} H_{z(n_{\text{TM}}^{\text{grv}})}^{\text{grv}\,\text{TE}}\Big] \tag{4b}$$

in which grv symbolizing "*groove*" may take on left, right, upp, or low. $\delta_{\text{grv,side}}$ is the Kronecker delta such that when grv $\equiv$ side (either left or right), it is unity, but zero otherwise, and likewise when grv $\equiv u\,\&\,\ell$ (either upp or low), $\delta_{\text{grv},u\,\&\,l}$ is unity, but zero otherwise. Now, coming to the crucial step; since the grooves are typically narrow, i.e., $g \ll \lambda$, it may be assumed that $n_{\text{TE}}^{\text{grv}} = 0$ and $n_{\text{TE}}^{\text{grv}} = 0$, leading to the existence of only the dominant $n_{\text{TE}}^{\text{grv}} = 0$ (TEM) mode and absence of all TM modes. As such, the $\vec{E}^{\text{grv}}$ in (3a) and (3c) is simply replaced by $\vec{E}_{n_{\text{TE}}^{\text{side}}=n_{\text{TM}}^{\text{side}}=0}^{\text{side}} = \hat{y} E_{y(n_{\text{TE}}^{\text{side}}=0)}^{\text{side}\,\text{TE}}$ when grv $\equiv$ side for the left and right grooves, and by $\vec{E}_{n_{\text{TE}}^{u\,\&\,\ell}=n_{\text{TM}}^{u\,\&\,\ell}=0}^{u\,\&\,\ell} = \hat{x} E_{x(n_{\text{TE}}^{u\,\&\,\ell}=0)}^{u\,\&\,\ell\,\text{TE}}$ when grv $\equiv u\,\&\,\ell$ for the upper and lower grooves. Hence, the only nonzero component of the E field within the groove is the one tangential to the corrugated surface and perpendicular to the grooves

and metal ridges. Similarly, the $\vec{H}^{\mathrm{grv}}$ in (3d) is reduced to $\vec{H}^{\mathrm{side}}_{n^{\mathrm{side}}_{\mathrm{TE}}=n^{\mathrm{side}}_{\mathrm{TM}}=0} = \hat{x}H^{\overset{\mathrm{side}}{\mathrm{TE}}}_{x(n^{\mathrm{side}}_{\mathrm{TE}}=0)} + \hat{z}H^{\overset{\mathrm{side}}{\mathrm{TE}}}_{z(n^{\mathrm{side}}_{\mathrm{TE}}=0)}$ when $\mathrm{grv} \equiv \mathrm{side}$ for the left and right grooves, and gets simplified to $\vec{H}^{u\,\&\,\ell}_{n^{u\,\&\,\ell}_{\mathrm{TE}}=n^{u\,\&\,\ell}_{\mathrm{TM}}=0} = \hat{y}H^{\overset{u\,\&\,\ell}{\mathrm{TE}}}_{y(n^{u\,\&\,\ell}_{\mathrm{TE}}=0)} + \hat{z}H^{\overset{u\,\&\,\ell}{\mathrm{TE}}}_{z(n^{u\,\&\,\ell}_{\mathrm{TE}}=0)}$ when $\mathrm{grv} \equiv u\,\&\,\ell$ for the upper and lower grooves. This means that only the axial component of the H field along the metallic ridges within the groove and the one perpendicular to the corrugated surface are existent, i.e., nonzero.

For all four corrugated surfaces, it is easily seen that (3a) is already satisfied upon setting the modal index $n^{\mathrm{grv}}_{T\psi}$ to zero. Thus, only three active ACBC equations remain: (3b)–(3d).

1) Right and Left Groove Interfaces With Central Region: $x = \pm a$*:* Equations(3b)–(3d) require

$$E^{\overset{\mathrm{cen}}{\mathrm{TE}^x}}_z(x=\mp a) + E^{\overset{\mathrm{cen}}{\mathrm{TM}^x}}_z(x=\mp a) = 0 \tag{5a}$$

$$E^{\overset{\{\mathrm{side}\}}{\mathrm{TE}}}_{y(n^{\{\mathrm{side}\}}_{\mathrm{TE}}=0)}(x=\mp a) = E^{\overset{\mathrm{cen}}{\mathrm{TE}^x}}_y(x=\mp a) + E^{\overset{\mathrm{cen}}{\mathrm{TM}^x}}_y(x=\mp a) \tag{5b}$$

$$H^{\overset{\{\mathrm{side}\}}{\mathrm{TE}}}_{z(n^{\{\mathrm{side}\}}_{\mathrm{TE}}=0)}(x=\mp a) = H^{\overset{\mathrm{cen}}{\mathrm{TE}^x}}_z(x=\mp a) + H^{\overset{\mathrm{cen}}{\mathrm{TM}^x}}_z(x=\mp a) \tag{5c}$$

in which $\{\mathrm{side}\} \equiv \{^{\mathrm{left}}_{\mathrm{right}}\}$, where the upper and lower items in the curly braces correspond to the upper and lower signs of $\mp$, pertaining to the left and right interfaces at $x = -a$ and $+a$, respectively.

Writing out (5a)–(5c) explicitly,

$$\begin{aligned}
&k^{\mathrm{cen}}_{y_{\mathrm{univ}}}\left(\zeta^{\overset{\mathrm{cen}}{\mathrm{TE}^x}}_{x_{\cos}} C^{\mathrm{cen}}_{x_{\mathrm{univ}}}\Big|_a \mp \zeta^{\overset{\mathrm{cen}}{\mathrm{TE}^x}}_{x_{\sin}} S^{\mathrm{cen}}_{x_{\mathrm{univ}}}\Big|_a\right)\\
&\quad\times\left(\zeta^{\overset{\mathrm{cen}}{\mathrm{TE}^x}}_{y_{\sin}} C^{\mathrm{cen}}_{y_{\mathrm{univ}}}\Big|_y - \zeta^{\overset{\mathrm{cen}}{\mathrm{TE}^x}}_{y_{\cos}} S^{\mathrm{cen}}_{y_{\mathrm{univ}}}\Big|_y\right)\\
&\quad\mp\frac{k^{\mathrm{cen}}_{x_{\mathrm{univ}}}k^{\mathrm{univ}}_z}{\omega\mu_{\mathrm{cen}}}\\
&\quad\times\left[\begin{array}{l}\left(\zeta^{\overset{\mathrm{cen}}{\mathrm{TM}^x}}_{x_{\cos}} S^{\mathrm{cen}}_{x_{\mathrm{univ}}}\Big|_a \pm \zeta^{\overset{\mathrm{cen}}{\mathrm{TM}^x}}_{x_{\sin}} C^{\mathrm{cen}}_{x_{\mathrm{univ}}}\Big|_a\right)\times\cdots\\ \cdots\times\left(\zeta^{\overset{\mathrm{cen}}{\mathrm{TM}^x}}_{y_{\cos}} C^{\mathrm{cen}}_{y_{\mathrm{univ}}}\Big|_y + \zeta^{\overset{\mathrm{cen}}{\mathrm{TM}^x}}_{y_{\sin}} S^{\mathrm{cen}}_{y_{\mathrm{univ}}}\Big|_y\right)\end{array}\right]\\
&=0
\end{aligned} \tag{6a}$$

$$\begin{aligned}
&\pm\frac{jk^{\mathrm{univ}}_z}{\varepsilon_{\{\mathrm{side}\}}}\zeta^{\overset{\{\mathrm{side}\}}{\mathrm{TE}}}_{x_{\sin}}\zeta^{\overset{\{\mathrm{side}\}}{\mathrm{TE}}}_{y_{\cos}}\sin\left(k^{\{\mathrm{side}\}}_{x_{\mathrm{TE}}}d\right)\\
&\quad\times\sum_{i=-(N_{\mathrm{seg}}-1)/2}^{(N_{\mathrm{seg}}-1)/2}\left(\zeta^{\overset{\{\mathrm{side}\}}{\mathrm{exp}}}_{y_{\cos}} C^{\mathrm{cen}}_{y_{\mathrm{univ}}}\Big|_{ip_y} + \zeta^{\overset{\{\mathrm{side}\}}{\mathrm{exp}}}_{y_{\sin}} S^{\mathrm{cen}}_{y_{\mathrm{univ}}}\Big|_{ip_y}\right)\\
&\quad\times\Pi_y(y-ip_y)\\
&=\frac{\kappa_y jk^{\mathrm{univ}}_z}{\varepsilon_{\mathrm{cen}}}\left[\begin{array}{l}\left(\zeta^{\overset{\mathrm{cen}}{\mathrm{TE}^x}}_{x_{\cos}} C^{\mathrm{cen}}_{x_{\mathrm{univ}}}\Big|_a \mp \zeta^{\overset{\mathrm{cen}}{\mathrm{TE}^x}}_{x_{\sin}} S^{\mathrm{cen}}_{x_{\mathrm{univ}}}\Big|_a\right)\\ \times\left(\zeta^{\overset{\mathrm{cen}}{\mathrm{TE}^x}}_{y_{\cos}} C^{\mathrm{cen}}_{y_{\mathrm{univ}}}\Big|_y + \zeta^{\overset{\mathrm{cen}}{\mathrm{TE}^x}}_{y_{\sin}} S^{\mathrm{cen}}_{y_{\mathrm{univ}}}\Big|_y\right)\end{array}\right]\\
&\quad+\frac{\kappa_y k^{\mathrm{cen}}_{x_{\mathrm{univ}}}k^{\mathrm{cen}}_{y_{\mathrm{univ}}}}{j\omega\mu_{\mathrm{cen}}\varepsilon_{\mathrm{cen}}}\\
&\quad\times\left[\begin{array}{l}\left(\zeta^{\overset{\mathrm{cen}}{\mathrm{TM}^x}}_{x_{\sin}} C^{\mathrm{cen}}_{x_{\mathrm{univ}}}\Big|_a \pm \zeta^{\overset{\mathrm{cen}}{\mathrm{TM}^x}}_{x_{\cos}} S^{\mathrm{cen}}_{x_{\mathrm{univ}}}\Big|_a\right)\\ \times\left(\zeta^{\overset{\mathrm{cen}}{\mathrm{TM}^x}}_{y_{\sin}} C^{\mathrm{cen}}_{y_{\mathrm{univ}}}\Big|_y - \zeta^{\overset{\mathrm{cen}}{\mathrm{TM}^x}}_{y_{\cos}} S^{\mathrm{cen}}_{y_{\mathrm{univ}}}\Big|_y\right)\end{array}\right]
\end{aligned} \tag{6b}$$

$$\begin{aligned}
&-\frac{k^{\{\mathrm{side}\}}_{x_{\mathrm{TE}}}k^{\mathrm{univ}}_z}{\omega\mu_{\{\mathrm{side}\}}\varepsilon_{\{\mathrm{side}\}}}\zeta^{\overset{\{\mathrm{side}\}}{\mathrm{TE}}}_{x_{\sin}}\zeta^{\overset{\{\mathrm{side}\}}{\mathrm{TE}}}_{y_{\cos}}\cos\left(k^{\{\mathrm{side}\}}_{x_{\mathrm{TE}}}d\right)\\
&\quad\times\sum_{i=-(N_{\mathrm{seg}}-1)/2}^{(N_{\mathrm{seg}}-1)/2}\left(\zeta^{\overset{\{\mathrm{side}\}}{\mathrm{exp}}}_{y_{\cos}} C^{\mathrm{cen}}_{y_{\mathrm{univ}}}\Big|_{ip_y} + \zeta^{\overset{\{\mathrm{side}\}}{\mathrm{exp}}}_{y_{\sin}} S^{\mathrm{cen}}_{y_{\mathrm{univ}}}\Big|_{ip_y}\right)\\
&\quad\times\Pi_y(y-ip_y)\\
&=\mp\frac{k^{\mathrm{cen}}_{x_{\mathrm{univ}}}k^{\mathrm{univ}}_z}{\omega\mu_{\mathrm{cen}}\varepsilon_{\mathrm{cen}}}\left[\begin{array}{l}\left(\zeta^{\overset{\mathrm{cen}}{\mathrm{TE}^x}}_{x_{\cos}} S^{\mathrm{cen}}_{x_{\mathrm{univ}}}\Big|_a \pm \zeta^{\overset{\mathrm{cen}}{\mathrm{TE}^x}}_{x_{\sin}} C^{\mathrm{cen}}_{x_{\mathrm{univ}}}\Big|_a\right)\\ \times\left(\zeta^{\overset{\mathrm{cen}}{\mathrm{TE}^x}}_{y_{\cos}} C^{\mathrm{cen}}_{y_{\mathrm{univ}}}\Big|_y + \zeta^{\overset{\mathrm{cen}}{\mathrm{TE}^x}}_{y_{\sin}} S^{\mathrm{cen}}_{y_{\mathrm{univ}}}\Big|_y\right)\end{array}\right]\\
&\quad+\frac{k^{\mathrm{cen}}_{y_{\mathrm{univ}}}}{\mu_{\mathrm{cen}}}\left[\begin{array}{l}\left(\zeta^{\overset{\mathrm{cen}}{\mathrm{TM}^x}}_{x_{\cos}} C^{\mathrm{cen}}_{x_{\mathrm{univ}}}\Big|_a \mp \zeta^{\overset{\mathrm{cen}}{\mathrm{TM}^x}}_{x_{\sin}} S^{\mathrm{cen}}_{x_{\mathrm{univ}}}\Big|_a\right)\\ \times\left(\zeta^{\overset{\mathrm{cen}}{\mathrm{TM}^x}}_{y_{\cos}} S^{\mathrm{cen}}_{y_{\mathrm{univ}}}\Big|_y - \zeta^{\overset{\mathrm{cen}}{\mathrm{TM}^x}}_{y_{\sin}} C^{\mathrm{cen}}_{y_{\mathrm{univ}}}\Big|_y\right)\end{array}\right]
\end{aligned} \tag{6c}$$

with

$$\left[\begin{array}{l} C^{\mathrm{cen}}_{w_{\mathrm{univ}}}\Big|_w\\ S^{\mathrm{cen}}_{w_{\mathrm{univ}}}\Big|_w\end{array}\right] = \left[\begin{array}{l}\cos\left(k^{\mathrm{cen}}_{w_{\mathrm{univ}}}w\right)\\ \sin\left(k^{\mathrm{cen}}_{w_{\mathrm{univ}}}w\right)\end{array}\right], \qquad w = x \text{ or } y \tag{7}$$

as modified from (2c) earlier, and whereby all $k^{\mathrm{cen}}_{w_{T\psi x}}$ in which ψ is E or M, w is x or y have been replaced by $k^{\mathrm{cen}}_{w_{\mathrm{univ}}}$, the universal phase constant (wavenumber component) along x or y shared by both TE and TM modes of the central region, i.e.,

$$k^{\mathrm{cen}}_{w_{T\psi x}} = k^{\mathrm{cen}}_{w_{\mathrm{univ}}} \tag{8a}$$

from which (2d) consequently becomes

$$k_{\mathrm{cen}} = \omega\sqrt{\mu_{\mathrm{cen}}\varepsilon_{\mathrm{cen}}} = \sqrt{\left(k^{\mathrm{cen}}_{x_{\mathrm{univ}}}\right)^2 + \left(k^{\mathrm{cen}}_{y_{\mathrm{univ}}}\right)^2 + \left(k^{\mathrm{univ}}_z\right)^2}. \tag{8b}$$

Also, in (6a)–(6c), a new factor κ_w has emerged (w may be x or y), being the correction factor applied only to the ACBC entailing the E-field components, defined as [24]

$$\kappa_w = p_w/g_w \quad w = x \text{ or } y. \tag{9}$$

A new summation term is incorporated to the left-hand sides (LHSs) of (6b) and (6c) (the explanation of which is to come) in which Π_w (w) is a unit pulse function of w (being x or y) having a width p_w (period along w) and centered at $w = 0$, i.e.,

$$\Pi_w(w) = \begin{cases} 1, & -p_w/2 < w < p_w/2\\ 0, & \text{otherwise.}\end{cases} \tag{10}$$

Thus, $\Pi_w(w - ip_w)$ is just this pulse function, but translated by $+ip_w$ along the w axis, where i is an integer. New coefficients $\zeta^{\overset{\{\mathrm{side}\}}{\mathrm{exp}}}_{y_{\cos}}$ and $\zeta^{\overset{\{\mathrm{side}\}}{\mathrm{exp}}}_{y_{\sin}}$ are also incorporated. Hence, the summations on the LHS of (6b) and (6c) describe how the fields within the grooves of the left and right corrugated walls vary with y in a discretized stepwise manner with each term of the summation being a piecewise constant within the ith groove, i.e., $ip_y - g_y/2 < y < ip_y + g_y/2$. This staircase variation is *forced to follow* the same trigonometric functional form as the variation with y in the central region with the same phase constant $k^{\mathrm{cen}}_{y_{\mathrm{univ}}}$, thus bearing the same harmonic for phase continuity. Those above-mentioned newly introduced coefficients

thus merely tag the discretized cosine and sine harmonic variations. This is termed as *discretized phase continuity*. Thus, this summation conveys the homogenization effect that has taken place when the entire corrugated region is perceived as just a single effective medium that is approximately homogeneous when "seen" macroscopically. The number of unit cells (segments) along the waveguide height is represented by N_{seg} (such that $p_y = 2b/N_{\text{seg}}$). It is reminded that $\{\text{side}\} \equiv \{^{\text{left}}_{\text{right}}\}$ in which the upper and lower items in the curly braces correspond to all sign pairs: $\pm$ and $\mp$ that appear in the same equation. Due to these sign pairs in every one of (6a)–(6c), there are thus a total of six distinct equations.

2) Upper and Lower Groove Interfaces With Central Region $y = \pm b$: Equations (3b)–(3d), respectively, require

$$E_z^{\overset{\text{cen}}{\text{TE}^x}}(y=\pm b) + E_z^{\overset{\text{cen}}{\text{TM}^x}}(y=\pm b) = 0 \tag{11a}$$

$$E^{\overset{\{u\,\&\,\ell\}}{\text{TE}}}_{x(n^{\{u\,\&\,\ell\}}_{\text{TE}}=0)}(y=\pm b) = E_x^{\overset{\text{cen}}{\text{TE}^x}}(y=\pm b) + E_x^{\overset{\text{cen}}{\text{TM}^x}}(y=\pm b) \tag{11b}$$

$$H^{\overset{\{u\,\&\,\ell\}}{\text{TE}}}_{z(n^{\{u\,\&\,\ell\}}_{\text{TE}}=0)}(y=\pm b) = H_z^{\overset{\text{cen}}{\text{TE}^x}}(y=\pm b) + H_z^{\overset{\text{cen}}{\text{TM}^x}}(y=\pm b) \tag{11c}$$

in which $\{u\,\&\,\ell\} \equiv \{^{\text{upp}}_{\text{low}}\}$, where as before, the upper and lower items in the curly braces correspond to the upper and lower signs of $\pm$, pertaining to the upper and lower interfaces at $y = b$ and $-b$, respectively.

Writing out (11a)–(11c) explicitly,

$$\begin{aligned}
&k^{\text{cen}}_{y_{\text{univ}}}\left(\zeta^{\overset{\text{cen}}{\text{TE}^x}}_{x_{\cos}} C^{\text{cen}}_{x_{\text{univ}}}\Big|_x + \zeta^{\overset{\text{cen}}{\text{TE}^x}}_{x_{\sin}} S^{\text{cen}}_{x_{\text{univ}}}\Big|_x\right)\\
&\quad\times\left(\zeta^{\overset{\text{cen}}{\text{TE}^x}}_{y_{\sin}} C^{\text{cen}}_{y_{\text{univ}}}\Big|_b \mp \zeta^{\overset{\text{cen}}{\text{TE}^x}}_{y_{\cos}} S^{\text{cen}}_{y_{\text{univ}}}\Big|_b\right)\\
&\quad+\frac{jk^{\text{cen}}_{x_{\text{univ}}}k^{\text{univ}}_z}{j\omega\mu_{\text{cen}}}\\
&\quad\times\left[\begin{array}{l}\left(\zeta^{\overset{\text{cen}}{\text{TM}^x}}_{x_{\cos}} S^{\text{cen}}_{x_{\text{univ}}}\Big|_x - \zeta^{\overset{\text{cen}}{\text{TM}^x}}_{x_{\sin}} C^{\text{cen}}_{x_{\text{univ}}}\Big|_x\right)\\ \times\left(\zeta^{\overset{\text{cen}}{\text{TM}^x}}_{y_{\cos}} C^{\text{cen}}_{y_{\text{univ}}}\Big|_b \pm \zeta^{\overset{\text{cen}}{\text{TM}^x}}_{y_{\sin}} S^{\text{cen}}_{y_{\text{univ}}}\Big|_b\right)\end{array}\right]\\
&=0
\end{aligned} \tag{12a}$$

$$\begin{aligned}
&\pm\frac{jk^{\text{univ}}_z}{\varepsilon_{\{u\,\&\,\ell\}}}\zeta^{\overset{\{u\,\&\,\ell\}}{\text{TE}}}_{x_{\cos}}\zeta^{\overset{\{u\,\&\,\ell\}}{\text{TE}}}_{y_{\sin}}\sin\left(k^{\{u\,\&\,\ell\}}_{y_{\text{TE}}}c\right)\\
&\quad\times\sum_{i=-(N_{\text{seg}}-1)/2}^{(N_{\text{seg}}-1)/2}\left(\zeta^{\overset{\{u\,\&\,\ell\}}{\text{exp}}}_{x_{\cos}} C^{\text{cen}}_{x_{\text{univ}}}\Big|_{ip_x} + \zeta^{\overset{\{u\,\&\,\ell\}}{\text{exp}}}_{x_{\sin}} S^{\text{cen}}_{x_{\text{univ}}}\Big|_{ip_x}\right)\Pi_x(x-ip_x)\\
&=\kappa_x\frac{k^2_{\text{cen}}-\left(k^{\text{cen}}_{x_{\text{univ}}}\right)^2}{j\omega\mu_{\text{cen}}\varepsilon_{\text{cen}}}\\
&\quad\times\left[\begin{array}{l}\left(\zeta^{\overset{\text{cen}}{\text{TM}^x}}_{x_{\cos}} C^{\text{cen}}_{x_{\text{univ}}}\Big|_x + \zeta^{\overset{\text{cen}}{\text{TM}^x}}_{x_{\sin}} S^{\text{cen}}_{x_{\text{univ}}}\Big|_x\right)\\ \times\left(\zeta^{\overset{\text{cen}}{\text{TM}^x}}_{y_{\cos}} C^{\text{cen}}_{y_{\text{univ}}}\Big|_b \pm \zeta^{\overset{\text{cen}}{\text{TM}^x}}_{y_{\sin}} S^{\text{cen}}_{y_{\text{univ}}}\Big|_b\right)\end{array}\right]
\end{aligned} \tag{12b}$$

$$\begin{aligned}
&-\frac{k^{\{u\,\&\,\ell\}}_{y_{\text{TE}}}k^{\text{univ}}_z}{\omega\mu_{\{u\,\&\,\ell\}}\varepsilon_{\{u\,\&\,\ell\}}}\zeta^{\overset{\{u\,\&\,\ell\}}{\text{TE}}}_{x_{\cos}}\zeta^{\overset{\{u\,\&\,\ell\}}{\text{TE}}}_{y_{\sin}}\cos\left(k^{\{u\,\&\,\ell\}}_{y_{\text{TE}}}c\right)\\
&\quad\times\sum_{i=-(N_{\text{seg}}-1)/2}^{(N_{\text{seg}}-1)/2}\left(\zeta^{\overset{\{u\,\&\,\ell\}}{\text{exp}}}_{x_{\cos}} C^{\text{cen}}_{x_{\text{univ}}}\Big|_{ip_x} + \zeta^{\overset{\{u\,\&\,\ell\}}{\text{exp}}}_{x_{\sin}} S^{\text{cen}}_{x_{\text{univ}}}\Big|_{ip_x}\right)\Pi_x(x-ip_x)\\
&=\frac{k^{\text{cen}}_{x_{\text{univ}}}k^{\text{univ}}_z}{\omega\mu_{\text{cen}}\varepsilon_{\text{cen}}}\left[\begin{array}{l}\left(\zeta^{\overset{\text{cen}}{\text{TE}^x}}_{x_{\cos}} S^{\text{cen}}_{x_{\text{univ}}}\Big|_x - \zeta^{\overset{\text{cen}}{\text{TE}^x}}_{x_{\sin}} C^{\text{cen}}_{x_{\text{univ}}}\Big|_x\right)\\ \times\left(\zeta^{\overset{\text{cen}}{\text{TE}^x}}_{y_{\cos}} C^{\text{cen}}_{y_{\text{univ}}}\Big|_b \pm \zeta^{\overset{\text{cen}}{\text{TE}^x}}_{y_{\sin}} S^{\text{cen}}_{y_{\text{univ}}}\Big|_b\right)\end{array}\right]\\
&\quad\pm\frac{k^{\text{cen}}_{y_{\text{univ}}}}{\mu_{\text{cen}}}\left[\begin{array}{l}\left(\zeta^{\overset{\text{cen}}{\text{TM}^x}}_{x_{\cos}} C^{\text{cen}}_{x_{\text{univ}}}\Big|_x + \zeta^{\overset{\text{cen}}{\text{TM}^x}}_{x_{\sin}} S^{\text{cen}}_{x_{\text{univ}}}\Big|_x\right)\\ \times\left(\zeta^{\overset{\text{cen}}{\text{TM}^x}}_{y_{\cos}} S^{\text{cen}}_{y_{\text{univ}}}\Big|_b \mp \zeta^{\overset{\text{cen}}{\text{TM}^x}}_{y_{\sin}} C^{\text{cen}}_{y_{\text{univ}}}\Big|_b\right)\end{array}\right]
\end{aligned} \tag{12c}$$

in which (7)–(10) and all the explanations that followed (6a)–(6c) reapply here. It is again reiterated that $\{u\,\&\,\ell\} \equiv \{^{\text{upp}}_{\text{low}}\}$ in which the upper and lower items in the curly braces correspond to all sign pairs: $\pm$ and $\mp$ that appear in the same equation. As was for (6a)–(6c), due to these sign pairs, a total of six individual equations are manifested by (12a)–(12c). Hence, there is a combined total of 12 equations conveyed by (6a)–(6c) and (12a)–(12c).

Every cosine and sine functional term (either in x or y) in these 12 equations is then decomposed into its two exponential components (each with opposite sign of its exponent from the other). The coefficients sharing the same form of exponential component are then grouped together. Subsequently, each of the resulting 12 equations is split into two, one for each exponential kernel term (plus or minus sign of the exponent), yielding a grand total of 24 distinct equations. The summation terms on the LHS of (6b), (6c), (12b), and (12c) originally represented discretized sinusoidal (cosine and sine) variations of the fields inside the homogenized corrugated region with y [for (6b) and (6c)] and x [for (12b) and (12c)]. Upon the aforesaid procedure of splitting each equation into its two exponential components, they become likewise staircase approximations (in each of the 16 equations that involve those summations), but this time, of exponential (instead of sinusoidal) variations of the fields. As the periods p_x and p_y tend to zero, those stepwise models of exponential functions then transform into continuous ones, which can then be canceled out with the exponential functional terms on the other (right-hand) side of each equation that are associated with the field variations within the central region, which have all along been of the continuous form, thereby simplifying the expressions. Consequently, for each pair of split equations (total of 12 pairs), the sum and difference of the two equations are taken, yielding back two equations.

C. Construction of Matrix Systems

Recapitulating from Section II-B, splitting each of the 12 equations conveyed by (6a)–(6c) and (12a)–(12c) into two yielded a grand total of 24 equations; 12 from the former three equations, 12 from the latter. Taking first the 12 equations of (6a)–(6c) pertaining to the ACBC equations for the left and

right interfaces ($x = -a$ and a) involving likewise 12 amplitude coefficients, a 12×12 homogeneous matrix equation can be constructed as follows:

$$\left[M_{ij}^{\ell\,\&\,r}\right]_{12\times 12}\left[\zeta_j^{\ell\,\&\,r}\right]_{12\times 1} = [0]_{12\times 1} \tag{13a}$$

in which the $\ell\,\&\,r$ superscript denotes left and right, and where the 12 coefficients of the column vector $[\zeta_j^{\ell\,\&\,r}]_{12\times 1}$ are

$$\begin{aligned}
\zeta_1^{\ell\,\&\,r} &= \zeta_{x_{\cos}}^{\mathrm{cen}\,\mathrm{TE}^x}\zeta_{y_{\cos}}^{\mathrm{cen}\,\mathrm{TE}^x}\\
\zeta_2^{\ell\,\&\,r} &= \zeta_{x_{\cos}}^{\mathrm{cen}\,\mathrm{TE}^x}\zeta_{y_{\sin}}^{\mathrm{cen}\,\mathrm{TE}^x}\\
\zeta_3^{\ell\,\&\,r} &= \zeta_{x_{\sin}}^{\mathrm{cen}\,\mathrm{TE}^x}\zeta_{y_{\cos}}^{\mathrm{cen}\,\mathrm{TE}^x}\\
\zeta_4^{\ell\,\&\,r} &= \zeta_{x_{\sin}}^{\mathrm{cen}\,\mathrm{TE}^x}\zeta_{y_{\sin}}^{\mathrm{cen}\,\mathrm{TE}^x}\\
\zeta_5^{\ell\,\&\,r} &= \zeta_{x_{\cos}}^{\mathrm{cen}\,\mathrm{TM}^x}\zeta_{y_{\cos}}^{\mathrm{cen}\,\mathrm{TM}^x}\\
\zeta_6^{\ell\,\&\,r} &= \zeta_{x_{\cos}}^{\mathrm{cen}\,\mathrm{TM}^x}\zeta_{y_{\sin}}^{\mathrm{cen}\,\mathrm{TM}^x}\\
\zeta_7^{\ell\,\&\,r} &= \zeta_{x_{\sin}}^{\mathrm{cen}\,\mathrm{TM}^x}\zeta_{y_{\cos}}^{\mathrm{cen}\,\mathrm{TM}^x}\\
\zeta_8^{\ell\,\&\,r} &= \zeta_{x_{\sin}}^{\mathrm{cen}\,\mathrm{TM}^x}\zeta_{y_{\sin}}^{\mathrm{cen}\,\mathrm{TM}^x}\\
\zeta_9^{\ell\,\&\,r} &= \zeta_{x_{\sin}}^{\mathrm{left}\,\mathrm{TE}}\zeta_{y_{\cos}}^{\mathrm{left}\,\mathrm{TE}}\zeta_{y_{\cos}}^{\mathrm{left}\,\mathrm{exp}}\\
\zeta_{10}^{\ell\,\&\,r} &= \zeta_{x_{\sin}}^{\mathrm{left}\,\mathrm{TE}}\zeta_{y_{\cos}}^{\mathrm{left}\,\mathrm{TE}}\zeta_{y_{\sin}}^{\mathrm{left}\,\mathrm{exp}}\\
\zeta_{11}^{\ell\,\&\,r} &= \zeta_{x_{\sin}}^{\mathrm{right}\,\mathrm{TE}}\zeta_{y_{\cos}}^{\mathrm{right}\,\mathrm{TE}}\zeta_{y_{\cos}}^{\mathrm{right}\,\mathrm{exp}}\\
\zeta_{12}^{\ell\,\&\,r} &= \zeta_{x_{\sin}}^{\mathrm{right}\,\mathrm{TE}}\zeta_{y_{\cos}}^{\mathrm{right}\,\mathrm{TE}}\zeta_{y_{\sin}}^{\mathrm{right}\,\mathrm{exp}}.
\end{aligned}$$

The matrix elements of $[M_{ij}^{\ell\,\&\,r}]$ are explicitly given in Appendix A.

Considering next the remaining 12 equations of (12a)–(12c) associated with the ACBC equations for the upper and lower interfaces ($y = b$ and $-b$) also entailing 12 amplitude coefficients, a second homogeneous 12×12 matrix equation may be obtained as

$$\left[M_{ij}^{u\,\&\,\ell}\right]_{12\times 12}\left[\zeta_j^{u\,\&\,\ell}\right]_{12\times 1} = [0]_{12\times 1} \tag{13b}$$

in which the $u\,\&\,\ell$ superscript denotes upper and lower, and where the first eight elements in the column vector $[\zeta_j^{u\,\&\,\ell}]_{12\times 1}$ are simply the same as those of $[M_{ij}^{\ell\,\&\,r}]$ earlier, i.e.,

$$\zeta_j^{u\,\&\,\ell} = \zeta_j^{\ell\,\&\,r}, \qquad \text{for } j = 1 \to 8 \tag{14}$$

and with the remaining four elements being

$$\begin{aligned}
\zeta_9^{u\,\&\,\ell} &= \zeta_{x_{\cos}}^{\mathrm{upp}\,\mathrm{TE}}\zeta_{y_{\sin}}^{\mathrm{upp}\,\mathrm{TE}}\zeta_{x_{\cos}}^{\mathrm{upp}\,\mathrm{exp}}\\
\zeta_{10}^{u\,\&\,\ell} &= \zeta_{x_{\cos}}^{\mathrm{upp}\,\mathrm{TE}}\zeta_{y_{\sin}}^{\mathrm{upp}\,\mathrm{TE}}\zeta_{x_{\sin}}^{\mathrm{upp}\,\mathrm{exp}}\\
\zeta_{11}^{u\,\&\,\ell} &= \zeta_{x_{\cos}}^{\mathrm{low}\,\mathrm{TE}}\zeta_{y_{\sin}}^{\mathrm{low}\,\mathrm{TE}}\zeta_{x_{\cos}}^{\mathrm{low}\,\mathrm{exp}}\\
\zeta_{12}^{u\,\&\,\ell} &= \zeta_{x_{\cos}}^{\mathrm{low}\,\mathrm{TE}}\zeta_{y_{\sin}}^{\mathrm{low}\,\mathrm{TE}}\zeta_{x_{\sin}}^{\mathrm{low}\,\mathrm{exp}}.
\end{aligned}$$

Likewise, the explicit matrix elements of $[M_{ij}^{u\,\&\,\ell}]$ are given in Appendix A.

D. Analytical Closed-Form Characteristic Dispersion Equation and Modal Resonance Search

By performing Gauss elimination on the matrices of (13a) and (13b), the row echelon form for both matrix equations may be obtained, from which the determinants of both matrices $[M_{ij}^{\ell\,\&\,r}]$ and $[M_{ij}^{u\,\&\,\ell}]$ are then acquired simply as the products of the diagonal elements. These two determinants, $\det[M_{ij}^{\ell\,\&\,r}]$ and $\det[M_{ij}^{u\,\&\,\ell}]$, are explicitly stated in Appendix C by (App-C1) and (App-C2). As such, closed-form analytical determinants of the matrices are obtained. By back substitution of the Gauss eliminated forms of both matrices, the modal coefficients are also acquired. Due to space constraints, their explicit forms are not provided, but they can be readily worked out from the given matrix elements of Appendix A.

In order for nontrivial solutions of the two matrix equations in (13a) and (13b), their determinants must vanish. When this occurs (i.e., $\det[M_{ij}^{\ell\,\&\,r}] \equiv \det[M_{ij}^{u\,\&\,\ell}] \equiv 0$) for the same set of parameters common to both matrix systems comprising the radian frequency ω and the pair of transverse wavenumbers for the central region $(k_{x_{\mathrm{univ}}}^{\mathrm{cen}}, k_{y_{\mathrm{univ}}}^{\mathrm{cen}})$, a single resonance condition under those parameters $(\omega_{\mathrm{res}}, k_{x_{\mathrm{univ}}}^{\mathrm{cen}}|_{\mathrm{res}}, k_{y_{\mathrm{univ}}}^{\mathrm{cen}}|_{\mathrm{res}})$ is obtained. These subsequently dictate the resonant axial propagation constant via (8b),

$$k_{z,\mathrm{res}}^{\mathrm{univ}} = \sqrt{\omega_{\mathrm{res}}^2\mu_{\mathrm{cen}}\varepsilon_{\mathrm{cen}} - \left(k_{x_{\mathrm{univ}}}^{\mathrm{cen}}\big|_{\mathrm{res}}\right)^2 - \left(k_{y_{\mathrm{univ}}}^{\mathrm{cen}}\big|_{\mathrm{res}}\right)^2} \tag{15}$$

which, in turn, determines the corresponding resonant wavenumber component within the groove region that is perpendicular to the corrugated surface, i.e., from (1j),

$$\begin{aligned}
k_{x_{\mathrm{TE}}}^{\{\mathrm{side}\}}\Big|_{\mathrm{res}} &= \sqrt{\omega_{\mathrm{res}}^2\mu_{\mathrm{side}}\varepsilon_{\mathrm{side}} - \left(k_z^{\mathrm{univ}}|_{\mathrm{res}}\right)^2}\\
k_{y_{\mathrm{TE}}}^{\mathrm{side}} &= \frac{n_{\mathrm{TE}}^{\mathrm{side}}\pi}{g_y} = 0 \qquad (16a)\\
k_{y_{\mathrm{TE}}}^{\{u\,\&\,\ell\}}\Big|_{\mathrm{res}} &= \sqrt{\omega_{\mathrm{res}}^2\mu_{u\,\&\,\ell}\varepsilon_{u\,\&\,\ell} - \left(k_z^{\mathrm{univ}}|_{\mathrm{res}}\right)^2}\\
k_{x_{\mathrm{TE}}}^{u\,\&\,\ell} &= \frac{n_{\mathrm{TE}}^{u\,\&\,\ell}\pi}{g_x} = 0. \qquad (16b)
\end{aligned}$$

The absolutes of both matrix determinants are then added together and equated to zero, thereby constituting the ultimate characteristic dispersion equation

$$\Omega\left(\omega, k_{x_{\mathrm{univ}}}^{\mathrm{cen}}, k_{y_{\mathrm{univ}}}^{\mathrm{cen}}\right) = \left|\det\left[M_{ij}^{\ell\,\&\,r}\right]\right| + \left|\det\left[M_{ij}^{u\,\&\,\ell}\right]\right| = 0 \tag{17}$$

which, for a certain $\omega = \omega_{\mathrm{res}}$, a numerical search for its associated resonant transverse wavenumbers $(k_{x_{\mathrm{univ}}}^{\mathrm{cen}}|_{\mathrm{res}}, k_{y_{\mathrm{univ}}}^{\mathrm{cen}}|_{\mathrm{res}})$ is conducted, which may be detected as sharp dips in the wire-frame mesh plots of $\log_{10}\ \Omega$ against the search ranges of $(k_{x_{\mathrm{univ}}}^{\mathrm{cen}}, k_{y_{\mathrm{univ}}}^{\mathrm{cen}})$, as will be demonstrated later in Section III.

E. Analytical Closed-Form Modal Field Functions in Various Regions

Upon detecting modal resonances, the analytical closed-form mathematical expressions of the eigen-modal vector field com-

ponents for the various regions may be written as follows, all of which pertain to the resonance condition characterized by $(\omega_{\rm res}, k^{\rm cen}_{x_{\rm univ}}|_{\rm res}, k^{\rm cen}_{y_{\rm univ}}|_{\rm res}; k^{\rm univ}_{z,{\rm res}})$.

1) Side (Left and Right) Corrugated Regions (Homogenized): The components of the fields within the side regions are stated as follows (all other components not listed are zero):

$$E_y^{\{\rm side\}}{}_{\rm TE} = \frac{jk^{\rm univ}_{z,{\rm res}}}{\varepsilon_{\{\rm side\}}} S^{\{\rm side\}}_{x_{\rm TE}} \Psi^{\{\rm side\}}_{\rm res}$$

$$H_x^{\{\rm side\}}{}_{\rm TE} = \frac{k^2_{\{\rm side\}\rm res} - \left(k^{\{\rm side\}}_{x_{\rm TE}}\Big|_{\rm res}\right)^2}{j\omega_{\rm res}\mu_{\{\rm side\}}\varepsilon_{\{\rm side\}}} S^{\{\rm side\}}_{x_{\rm TE}}\Big|_{\rm res} \Psi^{\{\rm side\}}_{\rm res}$$

$$H_z^{\{\rm side\}}{}_{\rm TE} = -\frac{k^{\{\rm side\}}_{x_{\rm TE}}\Big|_{\rm res} k^{\rm univ}_{z,{\rm res}} C^{\{\rm side\}}_{x_{\rm TE}}\Big|_{\rm res} \Psi^{\{\rm side\}}_{\rm res}}{\omega_{\rm res}\mu_{\{\rm side\}}\varepsilon_{\{\rm side\}}}$$

all with

$$\Psi^{\{\rm side\}}_{\rm res} = \left(\begin{Bmatrix} \zeta_9^{\ell\,\&\,r} \\ \zeta_{11}^{\ell\,\&\,r} \end{Bmatrix} C^{\rm cen}_{y_{\rm univ}}\Big|_y^{\rm res} + \begin{Bmatrix} \zeta_{10}^{\ell\,\&\,r} \\ \zeta_{12}^{\ell\,\&\,r} \end{Bmatrix} S^{\rm cen}_{y_{\rm univ}}\Big|_y^{\rm res} \right) e^{-jk^{\rm univ}_{z,{\rm res}}z}.$$

As before, $\{\rm side\} \equiv \{^{\rm left}_{\rm right}\}$, whose upper and lower scripts correspond to those within other curly braces in the same equation, and all res scripts symbolize that their associated quantities pertain to the resonance condition.

2) Upper and Lower Corrugated Regions (Homogenized): Likewise, all other field components of the upper and lower regions that are not listed as follows are zero:

$$E_x^{\{u\,\&\,\ell\}}{}_{\rm TE} = -\frac{jk^{\rm univ}_{z,{\rm res}}}{\varepsilon_{\{u\,\&\,\ell\}}} S^{\{u\,\&\,\ell\}}_{y_{\rm TE}}\Big|_{\rm res} \Psi^{\{u\,\&\,\ell\}}_{\rm res}$$

$$H_y^{\{u\,\&\,\ell\}}{}_{\rm TE} = \frac{k^2_{\{u\,\&\,\ell\}\rm res} - \left(k^{\{u\,\&\,\ell\}}_{y_{\rm TE}}|_{\rm res}\right)^2}{j\omega_{\rm res}\mu_{\{u\,\&\,\ell\}}\varepsilon_{\{u\,\&\,\ell\}}} \times S^{\{u\,\&\,\ell\}}_{y_{\rm TE}}\Big|_{\rm res} \Psi^{\{u\,\&\,\ell\}}_{\rm res}$$

$$H_z^{\{u\,\&\,\ell\}}{}_{\rm TE} = -\frac{k^{\{u\,\&\,\ell\}}_{y_{\rm TE}}\Big|_{\rm res} k^{\rm univ}_{z,{\rm res}} C^{\{u\,\&\,\ell\}}_{y_{\rm TE}}\Big|_{\rm res} \Psi^{\{u\,\&\,\ell\}}_{\rm res}}{\omega_{\rm res}\mu_{\{u\,\&\,\ell\}}\varepsilon_{\{u\,\&\,\ell\}}}$$

$$\Psi^{\{u\,\&\,\ell\}}_{\rm res} = \left(\begin{Bmatrix} \zeta_9^{u\,\&\,\ell} \\ \zeta_{11}^{u\,\&\,\ell} \end{Bmatrix} C^{\rm cen}_{x_{\rm univ}}\Big|_x^{\rm res} + \begin{Bmatrix} \zeta_{10}^{u\,\&\,\ell} \\ \zeta_{12}^{u\,\&\,\ell} \end{Bmatrix} S^{\rm cen}_{x_{\rm univ}}\Big|_x^{\rm res} \right) e^{-jk^{\rm univ}_{z,{\rm res}}z}$$

where, as before, $\{u\,\&\,\ell\} \equiv \{^{\rm upp}_{\rm low}\}$, whose upper and lower scripts correspond to those within other curly braces in the same equation. Notice that no explicit form of $S^{\{u\,\&\,\ell\}}_{y_{\rm TE}}$ has been provided yet since it was only textually described earlier in Section II-A.1b [item v)] as a modification of (1gi) and (1gii).

3) Central Region: For the following field expressions of the central region, it is first declared that all superscripts (be it $\ell\,\&\,r$ or $u\,\&\,\ell$) have been dropped from the coefficients ζ_j for $j = 1$ to 8 in virtue of (14),

$$\begin{bmatrix} E_y^{\rm cen}{}_{\rm TE^x} \\ H_y^{\rm cen}{}_{\rm TM^x} \end{bmatrix} = \left\{ \frac{jk^{\rm univ}_{z,{\rm res}}}{\begin{bmatrix} \varepsilon_{\rm cen} \\ -\mu_{\rm cen} \end{bmatrix}} \right\}_{2\times1} \cdot \left\{ \begin{bmatrix} \zeta_1 & \zeta_2 & \zeta_3 & \zeta_4 \\ \zeta_5 & \zeta_6 & \zeta_7 & \zeta_8 \end{bmatrix} [\Phi]_{4\times1} \right\}_{2\times1}$$

$$\begin{bmatrix} E_z^{\rm cen}{}_{\rm TE^x} \\ H_z^{\rm cen}{}_{\rm TM^x} \end{bmatrix} = \left\{ \frac{k^{\rm cen}_{y_{\rm univ}}|_{\rm res}}{\begin{bmatrix} \varepsilon_{\rm cen} \\ -\mu_{\rm cen} \end{bmatrix}} \right\}_{2\times1} \cdot \left\{ \begin{bmatrix} \zeta_2 & -\zeta_1 & \zeta_4 & -\zeta_3 \\ \zeta_6 & -\zeta_5 & \zeta_8 & -\zeta_7 \end{bmatrix} [\Phi]_{4\times1} \right\}_{2\times1}$$

$$\begin{bmatrix} H_x^{\rm cen}{}_{\rm TE^x} \\ E_x^{\rm cen}{}_{\rm TM^x} \end{bmatrix} = \left\{ \frac{\omega^2_{\rm res}\mu_{\rm cen}\varepsilon_{\rm cen} - \begin{bmatrix} \left(k^{\rm cen}_{x_{\rm univ}}|_{\rm res}\right)^2 \\ \left(k^{\rm cen}_{y_{\rm univ}}|_{\rm res}\right)^2 \end{bmatrix}}{j\omega_{\rm res}\mu_{\rm cen}\varepsilon_{\rm cen}} \right\}_{2\times1} \cdot \left\{ \begin{bmatrix} \zeta_1 & \zeta_2 & \zeta_3 & \zeta_4 \\ \zeta_5 & \zeta_6 & \zeta_7 & \zeta_8 \end{bmatrix} [\Phi] \right\}_{2\times1}$$

$$\begin{bmatrix} H_y^{\rm cen}{}_{\rm TE^x} \\ E_y^{\rm cen}{}_{\rm TM^x} \end{bmatrix} = \frac{k^{\rm cen}_{x_{\rm univ}}|_{\rm res}\, k^{\rm cen}_{y_{\rm univ}}|_{\rm res}}{j\omega_{\rm res}\mu_{\rm cen}\varepsilon_{\rm cen}} \times \begin{bmatrix} \zeta_4 & -\zeta_3 & -\zeta_2 & \zeta_1 \\ \zeta_8 & -\zeta_7 & -\zeta_6 & \zeta_5 \end{bmatrix} [\Phi]$$

$$\begin{bmatrix} H_z^{\rm cen}{}_{\rm TE^x} \\ E_z^{\rm cen}{}_{\rm TM^x} \end{bmatrix} = \frac{k^{\rm cen}_{x_{\rm univ}}|_{\rm res}\, k^{\rm univ}_{z,{\rm res}}}{\omega_{\rm res}\mu_{\rm cen}\varepsilon_{\rm cen}} \times \begin{bmatrix} -\zeta_3 & -\zeta_4 & \zeta_1 & \zeta_2 \\ -\zeta_7 & -\zeta_8 & \zeta_5 & \zeta_6 \end{bmatrix} [\Phi]$$

$$\text{with} \quad [\Phi]_{4\times1} = \begin{bmatrix} C^{\rm cen}_{x_{\rm univ}}|^{\rm res}_x\, C^{\rm cen}_{y_{\rm univ}}|^{\rm res}_y \\ C^{\rm cen}_{x_{\rm univ}}|^{\rm res}_x\, S^{\rm cen}_{y_{\rm univ}}|^{\rm res}_y \\ S^{\rm cen}_{x_{\rm univ}}|^{\rm res}_x\, C^{\rm cen}_{y_{\rm univ}}|^{\rm res}_y \\ S^{\rm cen}_{x_{\rm univ}}|^{\rm res}_x\, S^{\rm cen}_{y_{\rm univ}}|^{\rm res}_y \end{bmatrix} e^{-jk^{\rm univ}_{z,{\rm res}}z}$$

and where the dot operator of the first three equations represents scalar multiplication between any two corresponding elements of two identically sized matrices, resulting in a matrix of that same size.

F. Various Wave-Type Regimes

Three types of modal waves can be analyzed with the present analysis; propagating fast space waves, propagating slow surface waves, and evanescent waves. Each of these are located in a separate regime in the dispersion diagram, as will be presented in Section II-F.1 for an arbitrary longitudinally corrugated rectangular waveguide.

1) Fast Space Waves: For this case, all $k^{\rm cen}_{x_{\rm univ}}|_{\rm res}, k^{\rm cen}_{y_{\rm univ}}|_{\rm res}$, and $k^{\rm univ}_{z,{\rm res}}$ are real, which from (15) means $(k^{\rm cen}_{x_{\rm univ}}|_{\rm res})^2 + (k^{\rm cen}_{y_{\rm univ}}|_{\rm res})^2 \le \omega^2_{\rm res}\mu_{\rm cen}\varepsilon_{\rm cen}$.

2) Slow Surface Waves: For this case, the positive real modal propagation constant $k^{\rm univ}_{z,{\rm res}}$ exceeds the wavenumber of the central region, $k_{\rm cen,res} = \omega_{\rm res}\sqrt{\mu_{\rm cen}\varepsilon_{\rm cen}}$, at the corresponding resonant frequency. Either both or just one of the two transverse modal wavenumbers, $k^{\rm cen}_{x_{\rm univ}}|_{\rm res}$ and $k^{\rm cen}_{y_{\rm univ}}|_{\rm res}$,

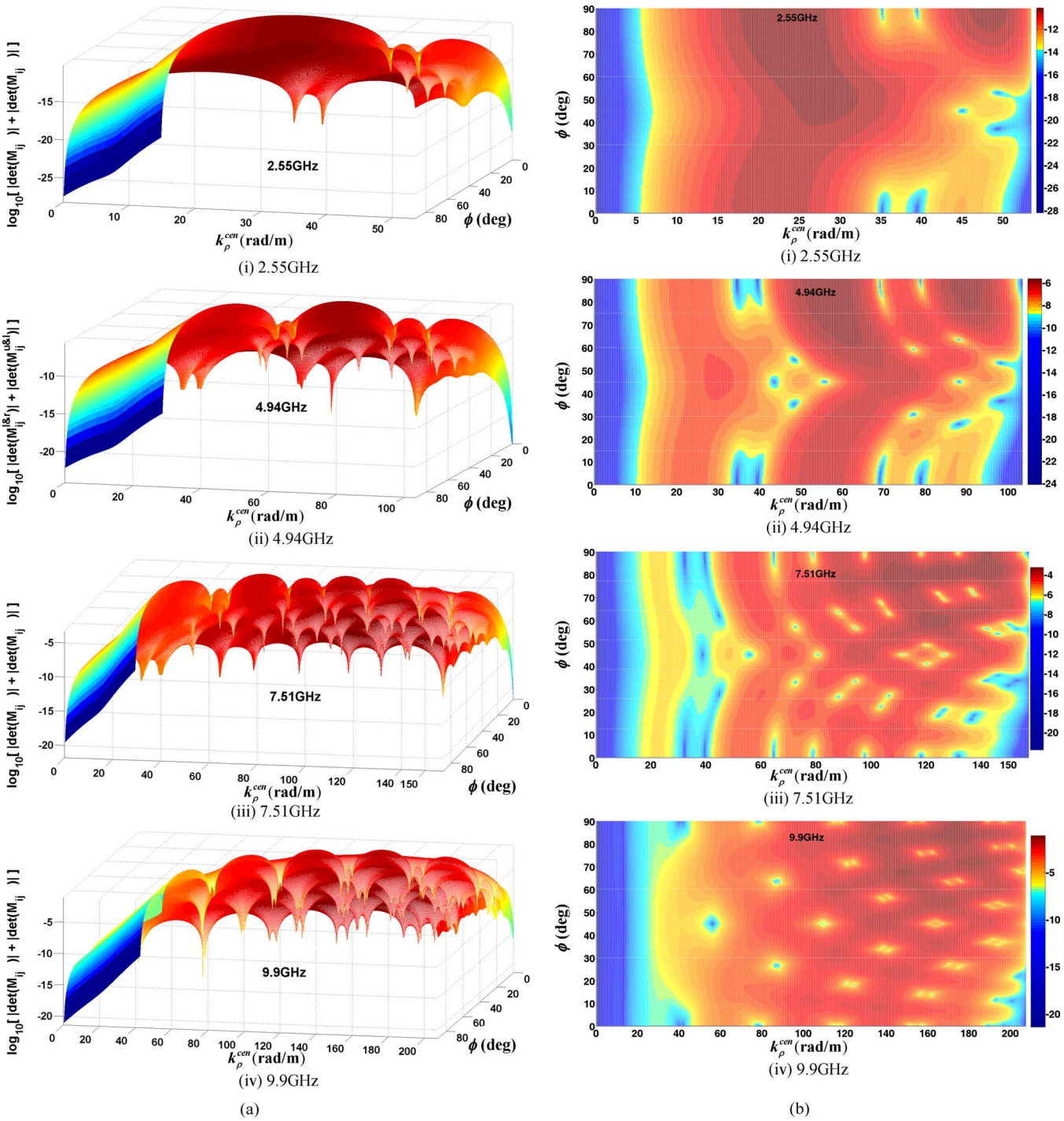

Fig. 2. (a) Wire-frame mesh plots of characteristic function $\log_{10}\Omega$ of (17) versus $k_\rho^{\rm cen}$ and ϕ for frequencies: (i) 2.55 GHz, (ii) 4.94 GHz, (iii) 7.51 GHz, and (iv) 9.9 GHz for $a = b = 40$ mm, $d = c = 4.15$ mm, $\varepsilon_{\rm cen} = \varepsilon_0, \mu_{\rm cen} = \mu_0, \varepsilon_{\rm left} = \varepsilon_{\rm right} = \varepsilon_{\rm upp} = \varepsilon_{\rm low} = 4.24\varepsilon_0, \mu_{\rm left} = \mu_{\rm right} = \mu_{\rm upp} = \mu_{\rm low} = \mu_0$, $p_x = p_y = 5$ mm, and $g_x/p_x = g_y/p_y = 0.9$. (b) Contour plots of characteristic function $\log_{10}\Omega$ of (17) versus $k_\rho^{\rm cen}$ and ϕ, for frequencies 2.55, 4.94, 7.51, and 9.9 GHz for $a = b = 40$ mm, $d = c = 4.15$ mm, $\varepsilon_{\rm cen} = \varepsilon_0, \mu_{\rm cen} = \mu_0, \varepsilon_{\rm left} = \varepsilon_{\rm right} = \varepsilon_{\rm upp} = \varepsilon_{\rm low} = 4.24\varepsilon_0, \mu_{\rm left} = \mu_{\rm right} = \mu_{\rm upp} = \mu_{\rm low} = \mu_0, p_x = p_y = 5$ mm, and $g_x/p_x = g_y/p_y = 0.9$.

may be imaginary, representative of decaying fields along the x and/or y direction perpendicular to the corrugated walls. When both transverse resonant wavenumbers are imaginary, $k_{x_{\rm univ}}^{\rm cen}|_{\rm res} = j\alpha_{x_{\rm univ}}^{\rm cen}|_{\rm res}$ & $k_{y_{\rm univ}}^{\rm cen}|_{\rm res} = j\alpha_{y_{\rm univ}}^{\rm cen}|_{\rm res}$; whereas, we may also have, say, $k_{x_{\rm univ}}^{\rm cen}|_{\rm res} = j\alpha_{x_{\rm univ}}^{\rm cen}|_{\rm res}$, but with $k_{y_{\rm univ}}^{\rm cen}|_{\rm res}$ remaining real.

3) Evanescent Waves: For this case, both $k_{x_{\rm univ}}^{\rm cen}|_{\rm res}$ and $k_{y_{\rm univ}}^{\rm cen}|_{\rm res}$ are real, but $k_{z,\rm res}^{\rm univ} = -j\alpha_{z,\rm res}^{\rm univ}$ is purely negative imaginary, meaning that

$$\left(k_{x_{\rm univ}}^{\rm cen}\Big|_{\rm res}\right)^2 + \left(k_{y_{\rm univ}}^{\rm cen}\Big|_{\rm res}\right)^2 > \omega_{\rm res}^2\mu_{\rm cen}\varepsilon_{\rm cen}.$$

III. Numerical Results

The randomly chosen parameters of an arbitrary axially corrugated rectangular waveguide to be showcased are first

stated as follows: $a = b = 40$ mm, $d = c = 4.15$ mm, and $\varepsilon_{\text{cen}} = \varepsilon_0, \mu_{\text{cen}} = \mu_0$, where ε_0 and μ_0 are the free-space permittivity and permeability, $\varepsilon_{\text{left}} = \varepsilon_{\text{right}} = \varepsilon_{\text{upp}} = \varepsilon_{\text{low}} = 4.24\varepsilon_0, \mu_{\text{left}} = \mu_{\text{right}} = \mu_{\text{upp}} = \mu_{\text{low}} = \mu_0$, with the number of unit cells (or periods) on any one corrugated wall being $N_{\text{seg}} = 16$ corresponding to a common period of $p_x = p_y = 2a/N_{\text{seg}} = 2b/N_{\text{seg}} = 5$ mm, and a universal groove width to period ratio of $g_w/p_w = 0.9$ for $w = x$ and y, associated with a likewise common groove width of $g_x = g_y = 4.5$ mm. The groove parameters correspond to a TEM hard frequency of about 10 GHz. Later on in Section III-C, computed results for another arbitrary set of parameters shall be presented.

A. Wireframe Mesh Plots of Characteristic Function

Fig. 2(a) shows the surface mesh plots of the characteristic function $\log_{10}\Omega$ of (17) versus the transverse radial wavenumber of the central region, $k_\rho^{\text{cen}} = \sqrt{(k_{x_{\text{univ}}}^{\text{cen}})^2 + (k_{y_{\text{univ}}}^{\text{cen}})^2}$, and the associated azimuth spectral angle, $\phi = \tan^{-1}(k_{y_{\text{univ}}}^{\text{cen}}/k_{x_{\text{univ}}}^{\text{cen}})$, for four randomly picked frequencies: 2.55, 4.94, 7.51, and 9.9 GHz. The corresponding contour thermal plots are given in Fig. 2(b).

Sharp dips indicative of eigen-modal resonances occurring at coordinates pertaining to $k_{\rho,\text{res}}^{\text{cen}} = \sqrt{(k_{x_{\text{univ}}}^{\text{cen}}|_{\text{res}})^2 + (k_{y_{\text{univ}}}^{\text{cen}}|_{\text{res}})^2}$ and $\phi_{\text{res}} = \tan^{-1}(k_{y_{\text{univ}}}^{\text{cen}}|_{\text{res}}/k_{x_{\text{univ}}}^{\text{cen}}|_{\text{res}})$ are evident in these plots. It is observed that these resonances occur symmetrically about the horizontal $\phi = 45°$ center line in Fig. 2(b). If perceived in the $k_{x_{\text{univ}}}^{\text{cen}} - k_{y_{\text{univ}}}^{\text{cen}}$ spectral coordinate system, this means that the resonant coordinates $(k_{x_{\text{univ}}}^{\text{cen}}|_{\text{res}}, k_{y_{\text{univ}}}^{\text{cen}}|_{\text{res}})$ are located symmetrically about the $\phi = 45°$ diagonal line, as expected of this waveguide example with a square cross section.

To appreciate how these dips came about, the contour thermal plots of $\log_{10}|\det(M_{ij}^{l\,\&\,r})|$ and $\log_{10}|\det(M_{ij}^{u\,\&\,l})|$ versus k_ρ^{cen} and ϕ for those same four arbitrary frequencies of Fig. 2 are presented as four pairs of plots in Fig. 3, each pertaining to a frequency, in which the upper plot of every pair is for $\log_{10}|\det(M_{ij}^{l\,\&\,r})|$, whereas the lower one is for $\log_{10}|\det(M_{ij}^{u\,\&\,l})|$. Contour paths corresponding to zero levels are clearly visible in each plot. For each frequency, i.e., a certain pair in Fig. 3, the coordinate locations pertaining to the intersections between the two sets of zero-level paths (one for $\log_{10}|\det(M_{ij}^{l\,\&\,r})|$, the other for $\log_{10}|\det(M_{ij}^{u\,\&\,l})|$) indeed tally up with the resonance points (sharp dips) of the contour plot associated with that frequency in Fig. 2(b). The zero-level contours of Fig. 3 clearly reveal that for every frequency, the "valleys" of both plots are mirror images of each other when one plot is placed on top of the other, as done in Fig. 3.

B. Dispersion Diagrams and Modal Field Distribution

The dispersion diagram for the corrugated waveguide parameters laid out at the start of this section generated according to the proposed methodology of Section II is presented in Fig. 4 as traces of dots, alongside which are traces of crosses representing the corresponding results simulated by the commercial full-wave solver CST Microwave Studio. Fig. 4(a) displays the propagating fast space and slow surface wave regimes,

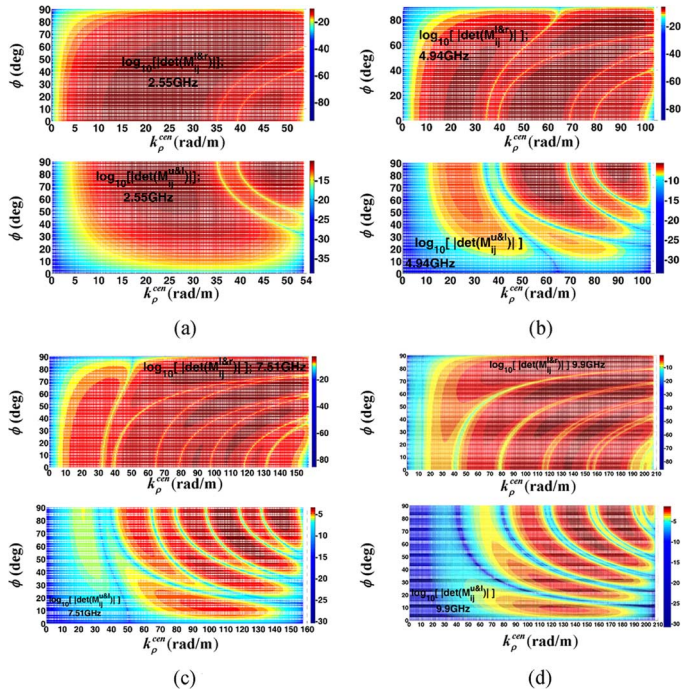

Fig. 3. Contour plots of $|\det(M_{ij}^{l\,\&\,r})|$ (upper graph for each frequency) and $|\det(M_{ij}^{u\,\&\,l})|$ (lower graph for each frequency) versus k_ρ^{cen} and ϕ for frequencies: (a) 2.55, (b) 4.94, (c) 7.51, and (d) 9.9 GHz. Same parameters as those of Fig. 2.

whereas Fig. 4(b) features the propagating fast space and evanescent wave regimes, the latter conveying the imaginary part of $k_{z,\text{res}}^{\text{univ}} = -j\alpha_{z,\text{res}}^{\text{univ}}$, i.e., $-\alpha_{z,\text{res}}^{\text{univ}}$, being the negative of the positive-valued attenuation constant. As observed, for all regimes, the modal dispersion traces of the present technique hold up well to those dictated by CST. Modal $|E|$-field distributions across the waveguide cross section at various frequencies indicated by arrows are also provided as inset plots in both Fig. 4(a) and (b), generated by both the present ACBC method and CST. The dominant modal fields are shown in Fig. 4(a), whereas those of the second-order mode are given in Fig. 4(b). The agreement of the modal field patterns between both approaches is also evident. At this juncture, it would also be worthwhile asserting that the ACBCs are accurate interface conditions capable of producing characteristic equations that embrace **all** modes.

For a clearer comparison between the modal field distributions obtained by the present analytical method and CST, graphs of the $|E|$-field versus either the width along x or height along y for planar cuts through $y = 0$ or $x = 0$, respectively, are given in Fig. 4(c). Field plots for the fundamental mode and the second most dominant one are provided. Good agreement between both approaches is clearly observed.

C. Another Arbitrary Example Set of Parameters

As a further illustration, the parameters of a second likewise random showcase of the axially corrugated rectangular waveguide are stated as follows. $a = b = 50$ mm, $d = c = 5$ mm, $\varepsilon_{\text{cen}} = \varepsilon_0, \mu_{\text{cen}} = \mu_0, \varepsilon_{\text{left}} = \varepsilon_{\text{right}} = \varepsilon_{\text{upp}} = \varepsilon_{\text{low}} = 10.2\varepsilon_0$, $\mu_{\text{left}} = \mu_{\text{right}} = \mu_{\text{upp}} = \mu_{\text{low}} = \mu_0, N_{\text{seg}} = 16$ with $p_x = p_y = 6.25$ mm, and $g_w/p_w = 0.6$ for $w = x$ and y

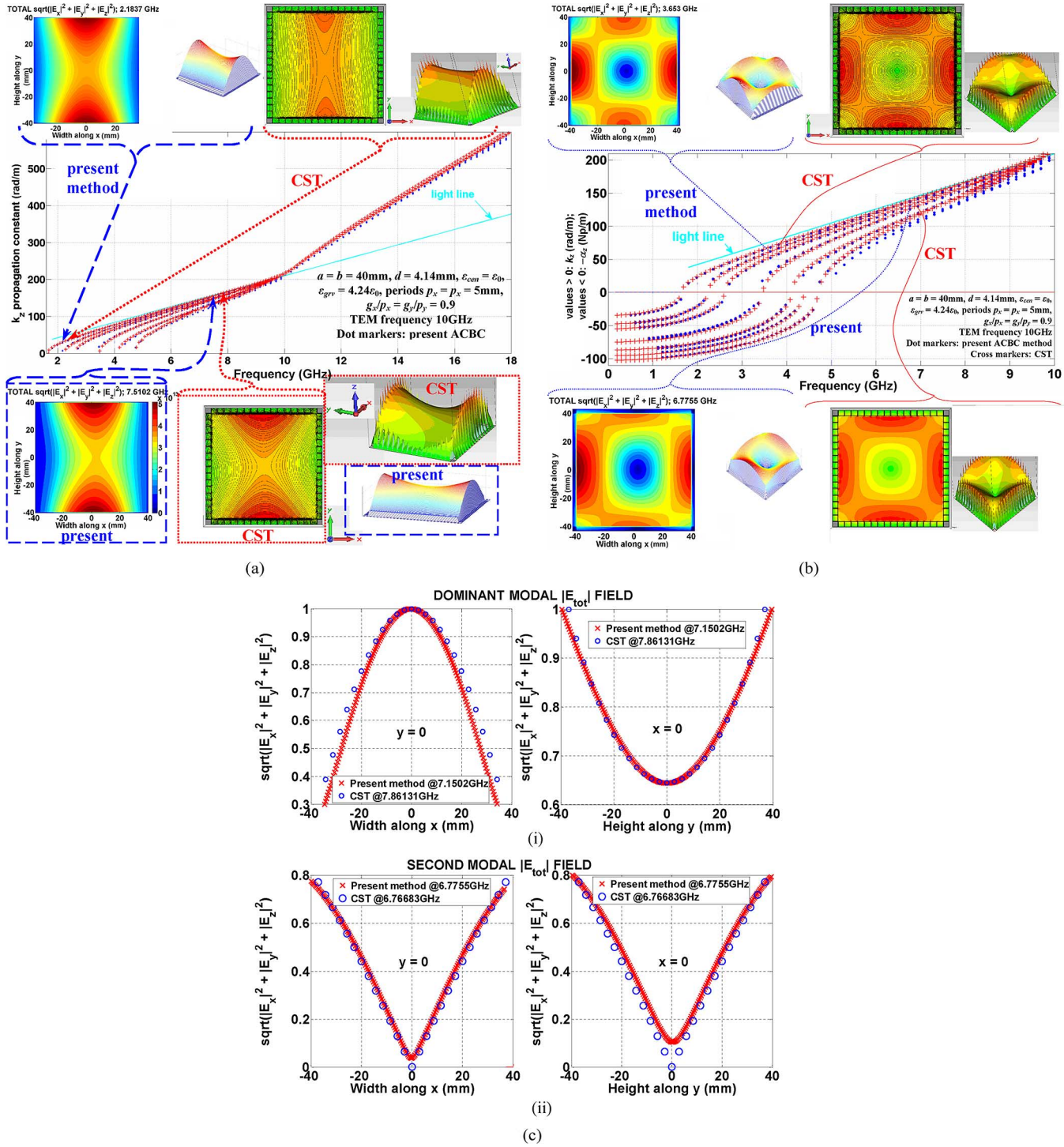

Fig. 4. (a) Dispersion by present ACBC approach (dot markers) and CST (cross markers) for propagating fast space wave and slow surface wave regimes. Same parameters as those of Fig. 2. $|E|$-field plots shown are for the **dominant** mode (with the highest propagation constant at any one frequency) at various frequencies indicated by arrows. (b) Dispersion by present ACBC approach (dot markers) and CST (cross markers) for propagating fast space wave and evanescent wave regimes. Same parameters as those of Fig. 2. $|E|$-field plots shown are for the **second** mode at various frequencies indicated by arrows. (c) Comparison between present ACBC method and CST of regular $|E|$-field plots for fixed plane-cuts through $y = 0$ (left-side plots) and $x = 0$ (right-side plots) for: (i) dominant mode and (ii) second mode.

pertaining to $g_x = g_y = 3.75$ mm. The groove parameters correspond this time to a TEM frequency of 4.94 GHz. As before, the dispersion modal curves for this set of parameters generated by the present formulation and by CST are shown in Fig. 5, this time with all three wave-type regimes (fast space, slow surface, and evanescent modal waves) being merged in a single graph. Once more, the fine agreement between both approaches is observed.

D. Approach to Conventional Homogeneous Waveguide as Groove Material Same as Central Medium and Corrugation Depth Tends to Zero

When the groove materials of all four grated walls are set the same as the medium occupying the central region of the corrugated waveguide, i.e., $\varepsilon_{\text{left}} = \varepsilon_{\text{right}} = \varepsilon_{\text{upp}} = \varepsilon_{\text{low}} = \varepsilon_{\text{cen}}$ with all equal permeabilities, and as all corrugation depths tend to zero, i.e., $d \to 0$ and $c \to 0$, the modal dispersion characteristics are expected to approach those of the resultant conventional homogeneously filled rectangular waveguide. With a width of w and height of h, the modal propagation constant of the (m, n)th mode for the latter waveguide uniformly occupied by a medium of parameters $(\mu_{\text{hom}}, \varepsilon_{\text{hom}})$ is given by

$$k_{z_{mn}}^{\text{hom}} = \sqrt{k_{\text{hom}}^2 - (m\pi/w)^2 - (n\pi/h)^2}$$
$$k_{\text{hom}} = \omega\sqrt{\mu_{\text{hom}}\varepsilon_{\text{hom}}}. \tag{18}$$

For $\varepsilon_{\text{cen}} = \varepsilon_0$ (and as are all groove permittivities) and $d = c = 0.5$ mm (a small corrugation depth), the dispersion curves for the corrugated waveguide with $a = b = 40$ mm, $\mu_{\text{cen}} = \mu_{\text{left}} = \mu_{\text{right}} = \mu_{\text{upp}} = \mu_{\text{low}} = \mu_0, p_x = p_y = 5$ mm, and $g_x/p_x = g_y/p_y = 0.9$ are given by Fig. 6 along with those of the corresponding empty waveguide with $w = 2a, h = 2b, \mu_{\text{hom}} = \mu_0$, and $\varepsilon_{\text{hom}} = \varepsilon_0$. Indeed, the modal traces of both structures virtually overlap as predicted.

As will be demonstrated in Section III-E, as long as the corrugation depth is small compared to the dimensions (a and b) of the central portion, the permittivity of the grooves does not actually have to be equal to that of the central region in order for the approach of the dispersion characteristics toward those of the conventional waveguide; the groove permittivity can actually assume any value by then (when the depth is small compared to the central region).

E. Computational Efficiency

The processing time of the present ACBC method coded up in MATLAB and that of the CST eigensolver, both run on an Intel Core i7-3820 CPU at 3.60-GHz clock speed and accompanied with 64.0 GB of RAM, were recorded for the same set of parameters as Figs. 2–4. For the ACBC approach, a total computational duration of 4207.96 s amounting to about 1 h, 10 min, and 8 s to obtain numerical data at 80 frequencies was observed, whereas the CST software took 4 h, 25 min, and 49 s in total on the same desktop computer for the same number of frequency points, slower by over 3 h! Even when the number of frequencies was reduced to just 30, the CST solver ran for 1 h, 35 min, and 1 s, still slower by about 25 min than the ACBC approach handling more than double the number of frequency points.

Therefore, not only is the present approach able to provide analytical field expressions as closed mathematical functions of the parameters, something that CST is incapable of, it is also immensely more computationally efficient.

F. Parametric Studies

The groove permittivity, $\varepsilon_{\text{left}} = \varepsilon_{\text{right}} = \varepsilon_{\text{upp}} = \varepsilon_{\text{low}}$, collectively represented by ε_{grv} for brevity, and the corrugation depth $d = c$ constitute the two parameters to be investigated. The parametric space for ε_{grv} comprises $2.24\varepsilon_0, 4.24\varepsilon_0$, and $6.24\varepsilon_0$, while $d = c$ spans over the values of 4.15, 8.15, and 12.15 mm, with the rest of the parameters remaining the same as those of Sections III-A and III-B (specifically, $a = b = 40$ mm, $\varepsilon_{\text{cen}} = \varepsilon_0, \mu_{\text{cen}} = \mu_{\text{left}} = \mu_{\text{right}} = \mu_{\text{upp}} = \mu_{\text{low}} = \mu_0, p_x = p_y = 5$ mm, and $g_x/p_x = g_y/p_y = 0.9$).

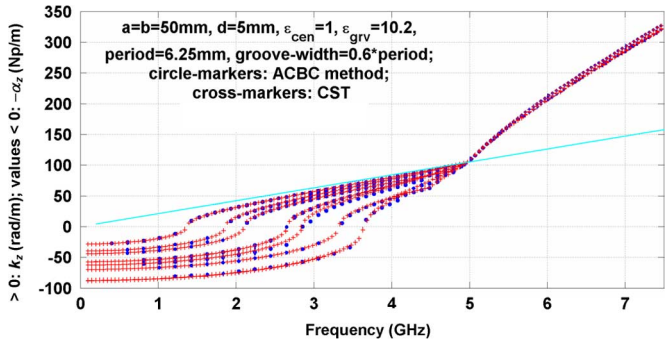

Fig. 5. Dispersion by present ACBC approach (dot markers) and CST (cross markers) for propagating fast space wave, slow surface wave, and evanescent wave regimes for $a = b = 50$ mm, $d = c = 5$ mm, $\varepsilon_{\text{cen}} = \varepsilon_0, \mu_{\text{cen}} = \mu_0$, $\varepsilon_{\text{left}} = \varepsilon_{\text{right}} = \varepsilon_{\text{upp}} = \varepsilon_{\text{low}} = 10.2\varepsilon_0, \mu_{\text{left}} = \mu_{\text{right}} = \mu_{\text{upp}} = \mu_{\text{low}} = \mu_0, p_x = p_y = 6.25$ mm, and $g_x/p_x = g_y/p_y = 0.6$.

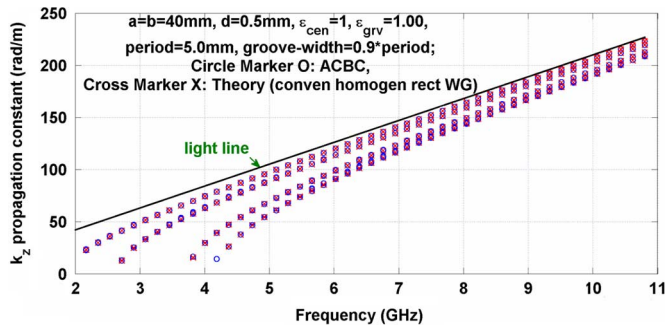

Fig. 6. Approach of dispersion toward conventional empty rectangular waveguide as groove material becomes vacuum and corrugation depth tends to zero. Circle markers: present ACBC approach, cross markers: theory by (18), for $a = b = 40$ mm, $d = c = 0.5$ mm, $\varepsilon_{\text{cen}} = \varepsilon_{\text{left}} = \varepsilon_{\text{right}} = \varepsilon_{\text{upp}} = \varepsilon_{\text{low}} = \varepsilon_0, \mu_{\text{cen}} = \mu_{\text{left}} = \mu_{\text{right}} = \mu_{\text{upp}} = \mu_{\text{low}} = \mu_0, p_x = p_y = 5$ mm, and $g_x/p_x = g_y/p_y = 0.9$.

The variation of the dominant modal dispersion behavior with the corrugation depth $d = c$ for the propagating fast space wave and evanescent wave regimes is conveyed by Fig. 7(a)–(c), each of them pertaining to a certain fixed value of ε_{grv} (the other parameter), namely, $2.24\varepsilon_0, 4.24\varepsilon_0$, and $6.24\varepsilon_0$, respectively. As observed, for each of all ε_{grv} cases, both the cutoff and TEM frequency (at which $k_z = k_0$) fall with increasing depth, and the modal trace translates leftward.

Swapping the fixed and varied parameters, Fig. 8(a)–(c) demonstrates how the dispersion varies with the groove permittivity ε_{grv}, each graph being associated with a controlled value of the other parameter, $d = c$, namely, 4.15, 8.15, and 12.15 mm, respectively. For each of the depth cases, both the cutoff and TEM frequencies fall with increasing ε_{grv}, and the modal trace translates leftward, all these being clearly visible only in Fig. 8(c), corresponding to the largest depth. The reduction of the cutoff frequency and leftward translation of the trace, however, show up only minutely in Fig. 8(b), pertaining

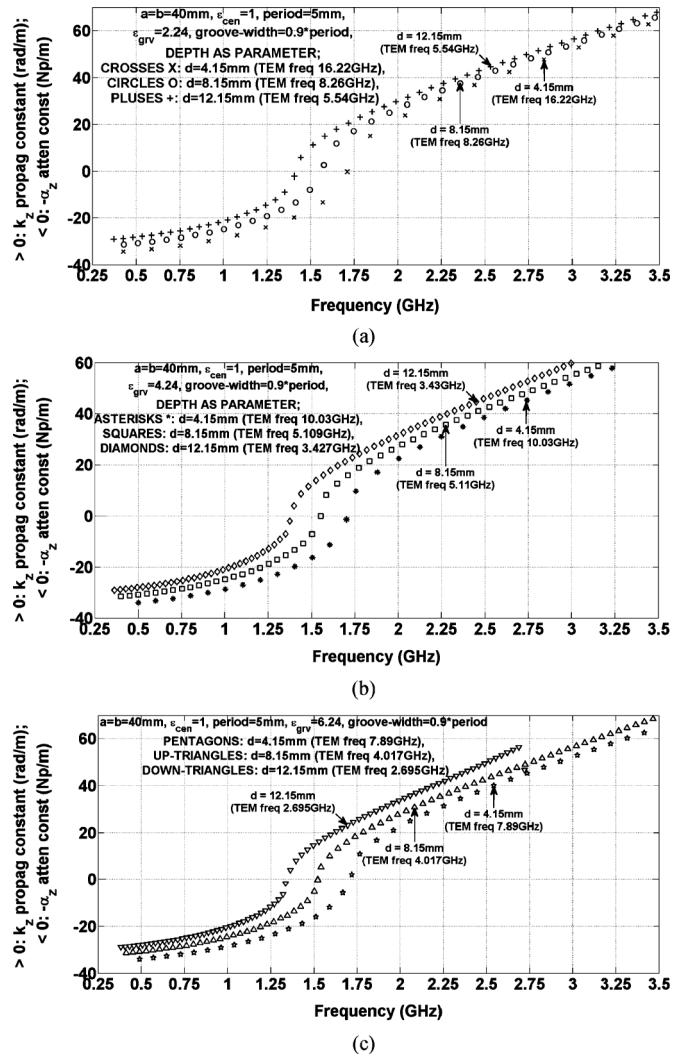

Fig. 7. Variation of dominant modal dispersion with **corrugation depth** $d = c$, for propagating fast space wave and evanescent wave regimes; $a = b = 40$ mm, $\varepsilon_{\rm cen} = \varepsilon_0$, $\mu_{\rm cen} = \mu_{\rm left} = \mu_{\rm right} = \mu_{\rm upp} = \mu_{\rm low} = \mu_0$, $p_x = p_y = 5$ mm, and $g_x/p_x = g_y/p_y = 0.9$ for $\varepsilon_{\rm grv} = \varepsilon_{\rm left} = \varepsilon_{\rm right} = \varepsilon_{\rm upp} = \varepsilon_{\rm low}$ equal to: (a) $2.24\varepsilon_0$, (b) $4.24\varepsilon_0$, and (c) $6.24\varepsilon_0$.

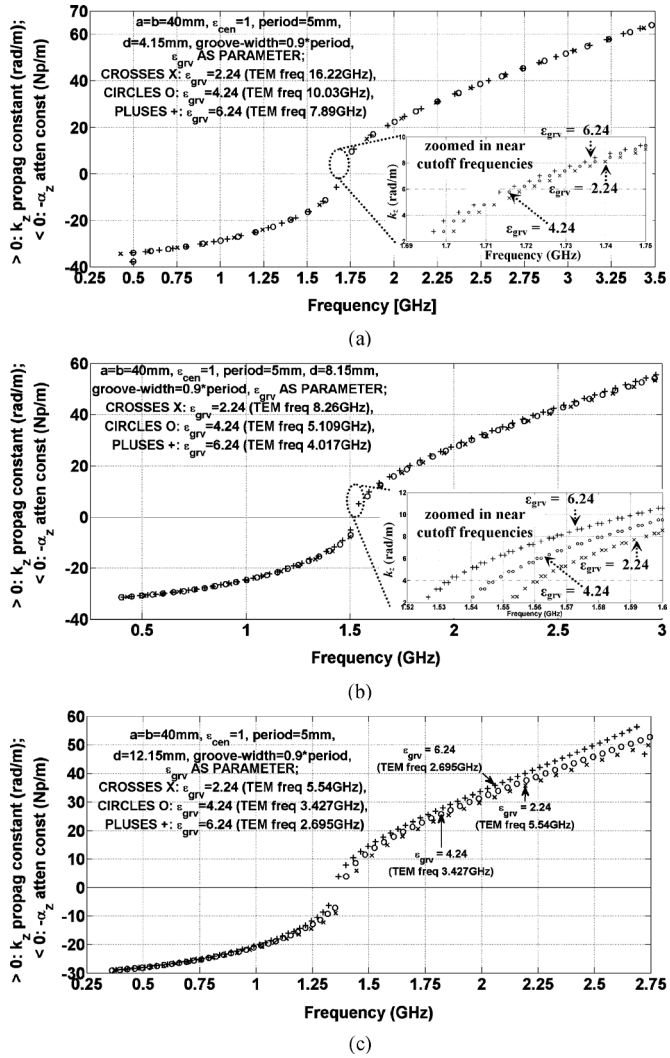

Fig. 8. Variation of dominant modal dispersion with **groove permittivity** $\varepsilon_{\rm grv} = \varepsilon_{\rm left} = \varepsilon_{\rm right} = \varepsilon_{\rm upp} = \varepsilon_{\rm low}$ for propagating fast space wave and evanescent wave regimes $a = b = 40$ mm, $\varepsilon_{\rm cen} = \varepsilon_0$, $\mu_{\rm cen} = \mu_{\rm left} = \mu_{\rm right} = \mu_{\rm upp} = \mu_{\rm low} = \mu_0$, $p_x = p_y = 5$ mm, $g_x/p_x = g_y/p_y = 0.9$ for corrugation depth $d = c$ equals to: (a) 4.15, (b) 8.15, and (c) 12.15 mm.

to a lower corrugation depth, being more apparent only from its inset plot zooming into frequencies near the cutoff frequency. By the point where the depth gets very small relative to the size of the central portion (via a and b) in Fig. 8(a), both those phenomena become virtually unnoticeable, albeit still visible upon closer inspection of the likewise inset zoomed-in plot. Hence, this leads to an important deduction: that the variations of the dispersion with the groove permittivity get more pronounced with increasing volumetric ratio of the corrugated region to the central portion. If this ratio is small, then it no longer matters what value $\varepsilon_{\rm grv}$ takes on as the effects of the large central portion dominate over those of the thinly grated walls (regardless of their groove-filling medium); the dispersion then approaches that of the conventional rectangular waveguide with cross-sectional size $2a \times 2b$ homogeneously filled by a medium of parameters $(\mu_{\rm cen}, \varepsilon_{\rm cen})$, just as though there are no corrugated walls, as demonstrated in Section III-D. As further information, the variations of the dominant modal cutoff frequency with the corrugation depth $d = c$ and groove permittivity are conveyed by Fig. 9.

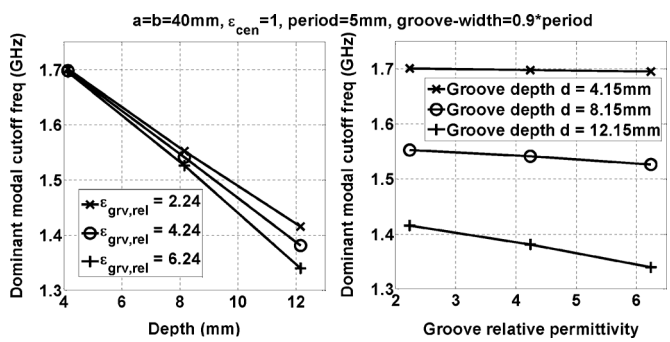

Fig. 9. Variation of dominant modal cutoff frequency with corrugation depth $d = c$ (*left*) and groove permittivity (*right*) $\varepsilon_{\rm grv} = \varepsilon_{\rm left} = \varepsilon_{\rm right} = \varepsilon_{\rm upp} = \varepsilon_{\rm low}$; $a = b = 40$ mm, $\varepsilon_{\rm cen} = \varepsilon_0$, $\mu_{\rm cen} = \mu_{\rm left} = \mu_{\rm right} = \mu_{\rm upp} = \mu_{\rm low} = \mu_0$, $p_x = p_y = 5$ mm, and $g_x/p_x = g_y/p_y = 0.9$.

G. Dielectric Losses of Groove Material

When dielectric losses of a medium are considered, its permittivity ε becomes complex with a positive real part ε' and a

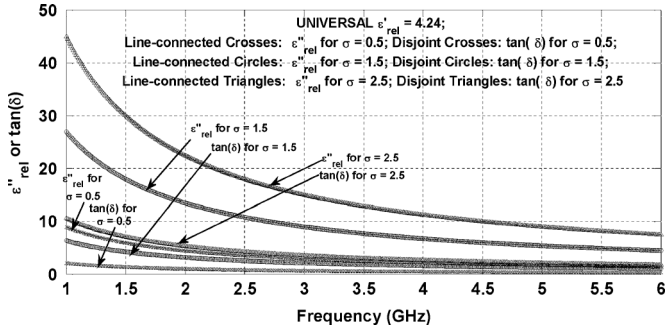

Fig. 10. Graph of $\varepsilon''_{\rm rel} = \varepsilon''/\varepsilon_0$ and $\tan\delta$ against frequency for various conductivities $\sigma = 0.5, 1.5$, and 2.5 or fixed real part $\varepsilon'_{\rm rel} = \varepsilon'/\varepsilon_0 = 4.24$ of the complex groove relative permittivity.

negative imaginary part $-\varepsilon''$, generally expressed as

$$\varepsilon = \varepsilon' - j\varepsilon'' = \varepsilon'(1 - j\tan\delta) \quad \tan\delta = \varepsilon''/\varepsilon' \tag{19a}$$

whereby $\tan\delta$ is the well-known loss tangent. An equivalent conductivity σ may alternatively be defined to represent all losses, being related to ε'' and the angular frequency $\omega = 2\pi f$ according to

$$\varepsilon'' = \sigma/\omega. \tag{19b}$$

Consequently, for a rectangular waveguide loaded with lossy dielectric media, both its transverse wavenumber components (k_x and k_y) and the axial propagation constant k_z become complex, the latter taking on the form of $\beta_z - j\alpha_z$ in which β_z and α_z are the positive-valued phase and attenuation constants, respectively.

Assuming $k^{\rm cen}_{y_{\rm univ}} = 0$ in the present context, thus considering modes with no variation along the y direction, the propagation constant of the corrugated waveguide is governed by

$$k_z^{\rm univ} = \beta_z - j\alpha_z = \sqrt{k_{\rm cen}^2 - \left(k^{\rm cen}_{x_{\rm univ}}\right)^2} \tag{20a}$$

$$k^{\rm cen}_{x_{\rm univ}} = \beta_x + j\alpha_x \tag{20b}$$

of which both β_x and α_x are positive real, thereby assuring that the complex $k_z^{\rm univ}$ falls in the fourth quadrant (both β_z and α_z positive), as required.

Substituting (20a) and (20b) into all preceding equations in Section II and with $k^{\rm cen}_{y_{\rm univ}} = 0$, the same $\Omega(\omega, \beta_x, \alpha_x)|_{k^{\rm cen}_{y_{\rm univ}}=0}$ as of (17) may be obtained, but this time as a function of β_x and α_x in addition to the angular frequency. In the same way as before, for a certain $\omega = \omega_{\rm res}$, a numerical search may be carried out, but now for the resonant $(\beta_x^{\rm res}, \alpha_x^{\rm res})$ coordinates, detected as sharp dips in the wire-frame mesh plots of $\log_{10}\Omega$ against the search ranges of $(\beta_x^{\rm res}, \alpha_x^{\rm res})$. The associated resonant $k_z^{\rm univ}|_{\rm res} = \beta_z^{\rm res} - j\alpha_z^{\rm res}$ may then be acquired using (20a) and (20b).

For a fixed value of 4.24 for the real part, $\varepsilon'_{\rm rel} = \varepsilon'/\varepsilon_0$, of the complex groove relative permittivity, three conductivity values are studied: $\sigma = 0.5$ S/m, 1.5 S/m, and 2.5 S/m. Associated with these values, the graphs of $\varepsilon''_{\rm rel} = \varepsilon''/\varepsilon_0$ and $\tan\delta$ are plotted against the frequency in Fig. 10 using (19a) and (19b).

Each pertaining to a particular mode and covering a certain band, Fig. 11(a)–(c) displays the graphs of the resonant α_z versus frequency for those three conductivities (the same parameters as in Sections III-A and III-B reapply). Evidently, the attenuation aggravates with increasing σ for all frequencies, as required.

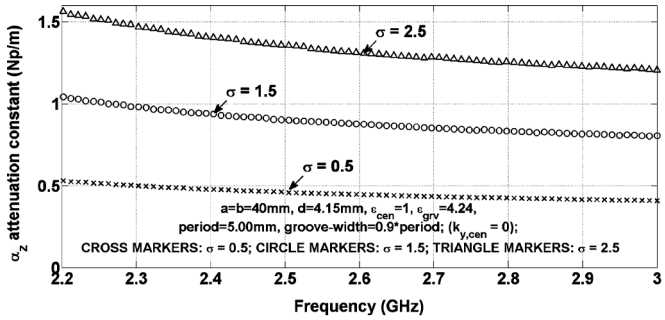

(a)

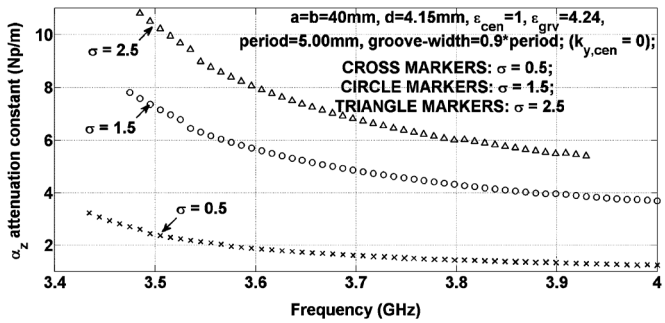

(b)

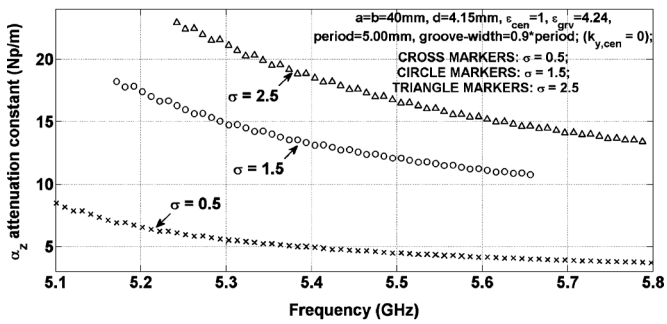

(c)

Fig. 11. Rise in attenuation constant with increasing conductivity through all frequencies; $a = b = 40$ mm, $d = c = 4.15$ mm, $\varepsilon_{\rm cen} = \varepsilon_0, \mu_{\rm cen} = \mu_0, \varepsilon_{\rm left} = \varepsilon_{\rm right} = \varepsilon_{\rm upp} = \varepsilon_{\rm low} = 4.24\varepsilon_0, \mu_{\rm left} = \mu_{\rm right} = \mu_{\rm upp} = \mu_{\rm low} = \mu_0, p_x = p_y = 5$ mm, and $g_x/p_x = g_y/p_y = 0.9$.

IV. Conclusion

This study has elegantly treated the axially corrugated rectangular waveguide analytically by vector potential modal analysis in tandem with the ACBC, thereby providing analytical modal field functions as well as the characteristic equation in closed-form expressions for all modal wave-types, i.e.: 1) fast propagating modal space-waves; 2) slow modal surface-waves; and 3) evanescent modes. Nowhere can all these be found elsewhere in the literature. By traditional analysis methods in their conventional forms, it is not possible to construct a solvable system of equations for the rectangular waveguide with all its four walls longitudinally corrugated. Revolutionary maneuvers are instead called upon to break out of this deadlock by considering two separate matrix systems of equations, each constructed

by the ACBCs for two opposite grated walls, and then combining them. Results of dispersion and modal field distributions yielded by this new method agree well with those generated by the commercial full-wave solver CST Microwave Studio. The modal analysis approach is also substantially more computationally efficient than the CST software. The availability of these mathematical forms for the modal fields empowers future researchers with the possibility of performing mode-matching analysis of such longitudinally corrugated waveguides when they are connected to other microwave devices.

Appendix A
Explicit Matrix Elements

In the following, all other matrix elements not listed are zero:

$$M^{\ell\&r}_{1,2} = k^{\mathrm{cen}}_{y_{\mathrm{univ}}}\ C^{\mathrm{cen}}_{x_{\mathrm{univ}}}\Big|_a$$
$$M^{\ell\&r}_{1,4} = -k^{\mathrm{cen}}_{y_{\mathrm{univ}}}\ S^{\mathrm{cen}}_{x_{\mathrm{univ}}}\Big|_a$$
$$M^{\ell\&r}_{1,5} = -\frac{k^{\mathrm{cen}}_{x_{\mathrm{univ}}} k^{\mathrm{univ}}_z}{\omega\mu_{\mathrm{cen}}}\ S^{\mathrm{cen}}_{x_{\mathrm{univ}}}\Big|_a$$
$$M^{\ell\&r}_{1,7} = -\frac{k^{\mathrm{cen}}_{x_{\mathrm{univ}}} k^{\mathrm{univ}}_z}{\omega\mu_{\mathrm{cen}}}\ C^{\mathrm{cen}}_{x_{\mathrm{univ}}}\Big|_a$$
$$M^{\ell\&r}_{2,1} = k^{\mathrm{cen}}_{y_{\mathrm{univ}}}\ C^{\mathrm{cen}}_{x_{\mathrm{univ}}}\Big|_a$$
$$M^{\ell\&r}_{2,3} = -k^{\mathrm{cen}}_{y_{\mathrm{univ}}}\ S^{\mathrm{cen}}_{x_{\mathrm{univ}}}\Big|_a$$
$$M^{\ell\&r}_{2,6} = \frac{k^{\mathrm{cen}}_{x_{\mathrm{univ}}} k^{\mathrm{univ}}_z}{\omega\mu_{\mathrm{cen}}}\ S^{\mathrm{cen}}_{x_{\mathrm{univ}}}\Big|_a$$
$$M^{\ell\&r}_{2,8} = \frac{k^{\mathrm{cen}}_{x_{\mathrm{univ}}} k^{\mathrm{univ}}_z}{\omega\mu_{\mathrm{cen}}}\ C^{\mathrm{cen}}_{x_{\mathrm{univ}}}\Big|_a$$
$$M^{\ell\&r}_{3,1} = \frac{\kappa_y j k^{\mathrm{univ}}_z\ C^{\mathrm{cen}}_{x_{\mathrm{univ}}}\Big|_a}{\varepsilon_{\mathrm{cen}}}$$
$$M^{\ell\&r}_{3,3} = -\frac{\kappa_y j k^{\mathrm{univ}}_z\ S^{\mathrm{cen}}_{x_{\mathrm{univ}}}\Big|_a}{\varepsilon_{\mathrm{cen}}}$$
$$M^{\ell\&r}_{3,6} = \frac{\kappa_y k^{\mathrm{cen}}_{x_{\mathrm{univ}}} k^{\mathrm{cen}}_{y_{\mathrm{univ}}}}{j\omega\mu_{\mathrm{cen}}\varepsilon_{\mathrm{cen}}}\ S^{\mathrm{cen}}_{x_{\mathrm{univ}}}\Big|_a$$
$$M^{\ell\&r}_{3,8} = \frac{\kappa_y k^{\mathrm{cen}}_{x_{\mathrm{univ}}} k^{\mathrm{cen}}_{y_{\mathrm{univ}}}}{j\omega\mu_{\mathrm{cen}}\varepsilon_{\mathrm{cen}}}\ C^{\mathrm{cen}}_{x_{\mathrm{univ}}}\Big|_a$$
$$M^{\ell\&r}_{3,9} = -\frac{j k^{\mathrm{univ}}_z}{\varepsilon_{\mathrm{left}}}\sin\left(k^{\mathrm{left}}_{x_{\mathrm{TE}}} d\right)$$
$$M^{\ell\&r}_{4,2} = -\frac{\kappa_y j k^{\mathrm{univ}}_z}{\varepsilon_{\mathrm{cen}}}\ C^{\mathrm{cen}}_{x_{\mathrm{univ}}}\Big|_a$$
$$M^{\ell\&r}_{4,4} = \frac{\kappa_y j k^{\mathrm{univ}}_z}{\varepsilon_{\mathrm{cen}}}\ S^{\mathrm{cen}}_{x_{\mathrm{univ}}}\Big|_a$$
$$M^{\ell\&r}_{4,5} = \frac{\kappa_y k^{\mathrm{cen}}_{x_{\mathrm{univ}}} k^{\mathrm{cen}}_{y_{\mathrm{univ}}}}{j\omega\mu_{\mathrm{cen}}\varepsilon_{\mathrm{cen}}}\ S^{\mathrm{cen}}_{x_{\mathrm{univ}}}\Big|_a$$
$$M^{\ell\&r}_{4,7} = \frac{\kappa_y k^{\mathrm{cen}}_{x_{\mathrm{univ}}} k^{\mathrm{cen}}_{y_{\mathrm{univ}}}}{j\omega\mu_{\mathrm{cen}}\varepsilon_{\mathrm{cen}}}\ C^{\mathrm{cen}}_{x_{\mathrm{univ}}}\Big|_a$$
$$M^{\ell\&r}_{4,10} = \frac{j k^{\mathrm{univ}}_z}{\varepsilon_{\mathrm{left}}}\sin\left(k^{\mathrm{left}}_{x_{\mathrm{TE}}} d\right)$$
$$M^{\ell\&r}_{5,1} = -\frac{k^{\mathrm{cen}}_{x_{\mathrm{univ}}} k^{\mathrm{univ}}_z}{\omega\mu_{\mathrm{cen}}\varepsilon_{\mathrm{cen}}}\ S^{\mathrm{cen}}_{x_{\mathrm{univ}}}\Big|_a$$
$$M^{\ell\&r}_{5,3} = -\frac{k^{\mathrm{cen}}_{x_{\mathrm{univ}}} k^{\mathrm{univ}}_z}{\omega\mu_{\mathrm{cen}}\varepsilon_{\mathrm{cen}}}\ C^{\mathrm{cen}}_{x_{\mathrm{univ}}}\Big|_a$$
$$M^{\ell\&r}_{5,6} = -\frac{k^{\mathrm{cen}}_{y_{\mathrm{univ}}}}{\mu_{\mathrm{cen}}}\ C^{\mathrm{cen}}_{x_{\mathrm{univ}}}\Big|_a$$
$$M^{\ell\&r}_{5,8} = \frac{k^{\mathrm{cen}}_{y_{\mathrm{univ}}}}{\mu_{\mathrm{cen}}}\ S^{\mathrm{cen}}_{x_{\mathrm{univ}}}\Big|_a$$
$$M^{\ell\&r}_{59} = \frac{k^{\mathrm{left}}_{x_{\mathrm{TE}}} k^{\mathrm{univ}}_z}{\omega\mu_{\mathrm{left}}\varepsilon_{\mathrm{left}}}\cos\left(k^{\mathrm{left}}_{x_{\mathrm{TE}}} d\right)$$
$$M^{\ell\&r}_{62} = \frac{k^{\mathrm{cen}}_{x_{\mathrm{univ}}} k^{\mathrm{univ}}_z}{\omega\mu_{\mathrm{cen}}\varepsilon_{\mathrm{cen}}}\ S^{\mathrm{cen}}_{x_{\mathrm{univ}}}\Big|_a$$
$$M^{\ell\&r}_{6,4} = \frac{k^{\mathrm{cen}}_{x_{\mathrm{univ}}} k^{\mathrm{univ}}_z}{\omega\mu_{\mathrm{cen}}\varepsilon_{\mathrm{cen}}}\ C^{\mathrm{cen}}_{x_{\mathrm{univ}}}\Big|_a$$
$$M^{\ell\&r}_{6,5} = -\frac{k^{\mathrm{cen}}_{y_{\mathrm{univ}}}}{\mu_{\mathrm{cen}}}\ C^{\mathrm{cen}}_{x_{\mathrm{univ}}}\Big|_a$$
$$M^{\ell\&r}_{6,7} = \frac{k^{\mathrm{cen}}_{y_{\mathrm{univ}}}}{\mu_{\mathrm{cen}}}\ S^{\mathrm{cen}}_{x_{\mathrm{univ}}}\Big|_a$$
$$M^{\ell\&r}_{6,10} = -\frac{k^{\mathrm{left}}_{x_{\mathrm{TE}}} k^{\mathrm{univ}}_z}{\omega\mu_{\mathrm{left}}\varepsilon_{\mathrm{left}}}\cos\left(k^{\mathrm{left}}_{x_{\mathrm{TE}}} d\right)$$
$$M^{\ell\&r}_{7,2} = k^{\mathrm{cen}}_{y_{\mathrm{univ}}}\ C^{\mathrm{cen}}_{x_{\mathrm{univ}}}\Big|_a$$
$$M^{\ell\&r}_{7,4} = k^{\mathrm{cen}}_{y_{\mathrm{univ}}}\ S^{\mathrm{cen}}_{x_{\mathrm{univ}}}\Big|_a$$
$$M^{\ell\&r}_{7,5} = \frac{k^{\mathrm{cen}}_{x_{\mathrm{univ}}} k^{\mathrm{univ}}_z\ S^{\mathrm{cen}}_{x_{\mathrm{univ}}}\Big|_a}{\omega\mu_{\mathrm{cen}}}$$
$$M^{\ell\&r}_{7,7} = -\frac{k^{\mathrm{cen}}_{x_{\mathrm{univ}}} k^{\mathrm{univ}}_z}{\omega\mu_{\mathrm{cen}}}\ C^{\mathrm{cen}}_{x_{\mathrm{univ}}}\Big|_a$$
$$M^{\ell\&r}_{8,1} = k^{\mathrm{cen}}_{y_{\mathrm{univ}}}\ C^{\mathrm{cen}}_{x_{\mathrm{univ}}}\Big|_a$$
$$M^{\ell\&r}_{8,3} = k^{\mathrm{cen}}_{y_{\mathrm{univ}}}\ S^{\mathrm{cen}}_{x_{\mathrm{univ}}}\Big|_a$$
$$M^{\ell\&r}_{8,6} = -\frac{k^{\mathrm{cen}}_{x_{\mathrm{univ}}} k^{\mathrm{univ}}_z\ S^{\mathrm{cen}}_{x_{\mathrm{univ}}}\Big|_a}{\omega\mu_{\mathrm{cen}}}$$
$$M^{\ell\&r}_{8,8} = \frac{k^{\mathrm{cen}}_{x_{\mathrm{univ}}} k^{\mathrm{univ}}_z\ C^{\mathrm{cen}}_{x_{\mathrm{univ}}}\Big|_a}{\omega\mu_{\mathrm{cen}}}$$
$$M^{\ell\&r}_{9,1} = \frac{\kappa_y j k^{\mathrm{univ}}_z\ C^{\mathrm{cen}}_{x_{\mathrm{univ}}}\Big|_a}{\varepsilon_{\mathrm{cen}}}$$
$$M^{\ell\&r}_{9,3} = \frac{\kappa_y j k^{\mathrm{univ}}_z\ S^{\mathrm{cen}}_{x_{\mathrm{univ}}}\Big|_a}{\varepsilon_{\mathrm{cen}}}$$
$$M^{\ell\&r}_{9,6} = \frac{\kappa_y j k^{\mathrm{cen}}_{x_{\mathrm{univ}}} k^{\mathrm{cen}}_{y_{\mathrm{univ}}}}{\omega\mu_{\mathrm{cen}}\varepsilon_{\mathrm{cen}}}\ S^{\mathrm{cen}}_{x_{\mathrm{univ}}}\Big|_a$$
$$M^{\ell\&r}_{9,8} = \frac{\kappa_y k^{\mathrm{cen}}_{x_{\mathrm{univ}}} k^{\mathrm{cen}}_{y_{\mathrm{univ}}}}{j\omega\mu_{\mathrm{cen}}\varepsilon_{\mathrm{cen}}}\ C^{\mathrm{cen}}_{x_{\mathrm{univ}}}\Big|_a$$
$$M^{\ell\&r}_{9,11} = \frac{j k^{\mathrm{univ}}_z \sin\left(k^{\mathrm{right}}_{x_{\mathrm{TE}}} d\right)}{\varepsilon_{\mathrm{right}}}$$
$$M^{\ell\&r}_{10,2} = \frac{\kappa_y k^{\mathrm{univ}}_z\ C^{\mathrm{cen}}_{x_{\mathrm{univ}}}\Big|_a}{j\varepsilon_{\mathrm{cen}}}$$
$$M^{\ell\&r}_{10,4} = \frac{\kappa_y k^{\mathrm{univ}}_z}{j\varepsilon_{\mathrm{cen}}}\ S^{\mathrm{cen}}_{x_{\mathrm{univ}}}\Big|_a$$
$$M^{\ell\&r}_{10,5} = \frac{\kappa_y j k^{\mathrm{cen}}_{x_{\mathrm{univ}}} k^{\mathrm{cen}}_{y_{\mathrm{univ}}}}{\omega\mu_{\mathrm{cen}}\varepsilon_{\mathrm{cen}}}\ S^{\mathrm{cen}}_{x_{\mathrm{univ}}}\Big|_a$$
$$M^{\ell\&r}_{10,7} = \frac{\kappa_y k^{\mathrm{cen}}_{x_{\mathrm{univ}}} k^{\mathrm{cen}}_{y_{\mathrm{univ}}}}{j\omega\mu_{\mathrm{cen}}\varepsilon_{\mathrm{cen}}}\ C^{\mathrm{cen}}_{x_{\mathrm{univ}}}\Big|_a$$

$$M^{\ell\&r}_{10,12} = \frac{k_z^{\text{univ}}}{j\varepsilon_{\text{right}}} \sin\left(k_{x_{\text{TE}}}^{\text{right}} d\right)$$

$$M^{\ell\&r}_{11,1} = \frac{k_{x_{\text{univ}}}^{\text{cen}} k_z^{\text{univ}}}{\omega\mu_{\text{cen}}\varepsilon_{\text{cen}}} \left. S_{x_{\text{univ}}}^{\text{cen}} \right|_a$$

$$M^{\ell\&r}_{11,3} = -\frac{k_{x_{\text{univ}}}^{\text{cen}} k_z^{\text{univ}}}{\omega\mu_{\text{cen}}\varepsilon_{\text{cen}}} \left. C_{x_{\text{univ}}}^{\text{cen}} \right|_a$$

$$M^{\ell\&r}_{11,6} = -\frac{k_{y_{\text{univ}}}^{\text{cen}}}{\mu_{\text{cen}}} \left. C_{x_{\text{univ}}}^{\text{cen}} \right|_a$$

$$M^{\ell\&r}_{11,8} = -\frac{k_{y_{\text{univ}}}^{\text{cen}}}{\mu_{\text{cen}}} \left. S_{x_{\text{univ}}}^{\text{cen}} \right|_a$$

$$M^{\ell\&r}_{11,11} = \frac{k_{x_{\text{TE}}}^{\text{right}} k_z^{\text{univ}}}{\omega\mu_{\text{right}}\varepsilon_{\text{right}}} \cos\left(k_{x_{\text{TE}}}^{\text{right}} d\right)$$

$$M^{\ell\&r}_{12,2} = -\frac{k_{x_{\text{univ}}}^{\text{cen}} k_z^{\text{univ}}}{\omega\mu_{\text{cen}}\varepsilon_{\text{cen}}} \left. S_{x_{\text{univ}}}^{\text{cen}} \right|_a$$

$$M^{\ell\&r}_{12,4} = \frac{k_{x_{\text{univ}}}^{\text{cen}} k_z^{\text{univ}}}{\omega\mu_{\text{cen}}\varepsilon_{\text{cen}}} \left. C_{x_{\text{univ}}}^{\text{cen}} \right|_a$$

$$M^{\ell\&r}_{12,5} = -\frac{k_{y_{\text{univ}}}^{\text{cen}}}{\mu_{\text{cen}}} \left. C_{x_{\text{univ}}}^{\text{cen}} \right|_a$$

$$M^{\ell\&r}_{12,7} = -\frac{k_{y_{\text{univ}}}^{\text{cen}}}{\mu_{\text{cen}}} \left. S_{x_{\text{univ}}}^{\text{cen}} \right|_a$$

$$M^{\ell\&r}_{12,12} = -\frac{k_{x_{\text{TE}}}^{\text{right}} k_z^{\text{univ}}}{\omega\mu_{\text{right}}\varepsilon_{\text{right}}} \cos\left(k_{x_{\text{TE}}}^{\text{right}} d\right)$$

$$M^{u\&\ell}_{1,1} = -k_{y_{\text{univ}}}^{\text{cen}} \left. S_{y_{\text{univ}}}^{\text{cen}} \right|_b$$

$$M^{u\&\ell}_{1,2} = k_{y_{\text{univ}}}^{\text{cen}} \left. C_{y_{\text{univ}}}^{\text{cen}} \right|_b$$

$$M^{u\&\ell}_{1,7} = -\frac{k_{x_{\text{univ}}}^{\text{cen}} k_z^{\text{univ}} \left. C_{y_{\text{univ}}}^{\text{cen}} \right|_b}{\omega\mu_{\text{cen}}}$$

$$M^{u\&\ell}_{1,8} = -\frac{k_{x_{\text{univ}}}^{\text{cen}} k_z^{\text{univ}} \left. S_{y_{\text{univ}}}^{\text{cen}} \right|_b}{\omega\mu_{\text{cen}}}$$

$$M^{u\&\ell}_{2,3} = -k_{y_{\text{univ}}}^{\text{cen}} \left. S_{y_{\text{univ}}}^{\text{cen}} \right|_b$$

$$M^{u\&\ell}_{2,4} = k_{y_{\text{univ}}}^{\text{cen}} \left. C_{y_{\text{univ}}}^{\text{cen}} \right|_b$$

$$M^{u\&\ell}_{2,5} = \frac{k_{x_{\text{univ}}}^{\text{cen}} k_z^{\text{univ}} \left. C_{y_{\text{univ}}}^{\text{cen}} \right|_b}{\omega\mu_{\text{cen}}}$$

$$M^{u\&\ell}_{2,6} = \frac{k_{x_{\text{univ}}}^{\text{cen}} k_z^{\text{univ}} \left. S_{y_{\text{univ}}}^{\text{cen}} \right|_b}{\omega\mu_{\text{cen}}}$$

$$M^{u\&\ell}_{3,5} = \kappa_x \frac{k_{\text{cen}}^2 - \left(k_{x_{\text{univ}}}^{\text{cen}}\right)^2}{j\omega\mu_{\text{cen}}\varepsilon_{\text{cen}}} \left. C_{y_{\text{univ}}}^{\text{cen}} \right|_b$$

$$M^{u\&\ell}_{3,6} = \kappa_x \frac{k_{\text{cen}}^2 - \left(k_{x_{\text{univ}}}^{\text{cen}}\right)^2}{j\omega\mu_{\text{cen}}\varepsilon_{\text{cen}}} \left. S_{y_{\text{univ}}}^{\text{cen}} \right|_b$$

$$M^{u\&\ell}_{3,9} = \frac{k_z^{\text{univ}} \sin\left(k_{y_{\text{TE}}}^{\text{upp}} c\right)}{j\varepsilon_{\text{upp}}}$$

$$M^{u\&\ell}_{4,7} = -\kappa_x \frac{k_{\text{cen}}^2 - \left(k_{x_{\text{univ}}}^{\text{cen}}\right)^2}{j\omega\mu_{\text{cen}}\varepsilon_{\text{cen}}} \left. C_{y_{\text{univ}}}^{\text{cen}} \right|_b$$

$$M^{u\&\ell}_{4,8} = -\kappa_x \frac{k_{\text{cen}}^2 - \left(k_{x_{\text{univ}}}^{\text{cen}}\right)^2}{j\omega\mu_{\text{cen}}\varepsilon_{\text{cen}}} \left. S_{y_{\text{univ}}}^{\text{cen}} \right|_b$$

$$M^{u\&\ell}_{4,10} = \frac{jk_z^{\text{univ}} \sin\left(k_{y_{\text{TE}}}^{\text{upp}} c\right)}{\varepsilon_{\text{upp}}}$$

$$M^{u\&\ell}_{5,3} = -\frac{k_{x_{\text{univ}}}^{\text{cen}} k_z^{\text{univ}} \left. C_{y_{\text{univ}}}^{\text{cen}} \right|_b}{\omega\mu_{\text{cen}}\varepsilon_{\text{cen}}}$$

$$M^{u\&\ell}_{5,4} = -\frac{k_{x_{\text{univ}}}^{\text{cen}} k_z^{\text{univ}} \left. S_{y_{\text{univ}}}^{\text{cen}} \right|_b}{\omega\mu_{\text{cen}}\varepsilon_{\text{cen}}}$$

$$M^{u\&\ell}_{5,5} = \frac{k_{y_{\text{univ}}}^{\text{cen}} \left. S_{y_{\text{univ}}}^{\text{cen}} \right|_b}{\mu_{\text{cen}}}$$

$$M^{u\&\ell}_{5,6} = -\frac{k_{y_{\text{univ}}}^{\text{cen}} \left. C_{y_{\text{univ}}}^{\text{cen}} \right|_b}{\mu_{\text{cen}}}$$

$$M^{u\&\ell}_{5,9} = \frac{k_{y_{\text{TE}}}^{\text{upp}} k_z^{\text{univ}} \cos\left(k_{y_{\text{TE}}}^{\text{upp}} c\right)}{\omega\mu_{\text{upp}}\varepsilon_{\text{upp}}}$$

$$M^{u\&\ell}_{6,1} = \frac{k_{x_{\text{univ}}}^{\text{cen}} k_z^{\text{univ}} \left. C_{y_{\text{univ}}}^{\text{cen}} \right|_b}{\omega\mu_{\text{cen}}\varepsilon_{\text{cen}}}$$

$$M^{u\&\ell}_{6,2} = \frac{k_{x_{\text{univ}}}^{\text{cen}} k_z^{\text{univ}} \left. S_{y_{\text{univ}}}^{\text{cen}} \right|_b}{\omega\mu_{\text{cen}}\varepsilon_{\text{cen}}}$$

$$M^{u\&\ell}_{6,7} = \frac{k_{y_{\text{univ}}}^{\text{cen}} \left. S_{y_{\text{univ}}}^{\text{cen}} \right|_b}{\mu_{\text{cen}}}$$

$$M^{u\&\ell}_{6,8} = -\frac{k_{y_{\text{univ}}}^{\text{cen}} \left. C_{y_{\text{univ}}}^{\text{cen}} \right|_b}{\mu_{\text{cen}}}$$

$$M^{u\&\ell}_{6,10} = \frac{k_{y_{\text{TE}}}^{\text{upp}} k_z^{\text{univ}} \cos\left(k_{y_{\text{TE}}}^{\text{upp}} c\right)}{\omega\mu_{\text{upp}}\varepsilon_{\text{upp}}}$$

$$M^{u\&\ell}_{7,1} = k_{y_{\text{TE}^x}}^{\text{cen}} \left. S_{y_{\text{univ}}}^{\text{cen}} \right|_b$$

$$M^{u\&\ell}_{7,2} = k_{y_{\text{univ}}}^{\text{cen}} \left. C_{y_{\text{univ}}}^{\text{cen}} \right|_b$$

$$M^{u\&\ell}_{7,7} = -\frac{k_{x_{\text{univ}}}^{\text{cen}} k_z^{\text{univ}} \left. C_{y_{\text{univ}}}^{\text{cen}} \right|_b}{\omega\mu_{\text{cen}}}$$

$$M^{u\&\ell}_{7,8} = \frac{k_{x_{\text{univ}}}^{\text{cen}} k_z^{\text{univ}} \left. S_{y_{\text{univ}}}^{\text{cen}} \right|_b}{\omega\mu_{\text{cen}}}$$

$$M^{u\&\ell}_{8,3} = k_{y_{\text{univ}}}^{\text{cen}} \left. S_{y_{\text{univ}}}^{\text{cen}} \right|_b$$

$$M^{u\&\ell}_{8,4} = k_{y_{\text{TE}^x}}^{\text{cen}} \left. C_{y_{\text{univ}}}^{\text{cen}} \right|_b$$

$$M^{u\&\ell}_{8,5} = \frac{k_{x_{\text{univ}}}^{\text{cen}} k_z^{\text{univ}} \left. C_{y_{\text{univ}}}^{\text{cen}} \right|_b}{\omega\mu_{\text{cen}}}$$

$$M^{u\&\ell}_{8,6} = -\frac{k_{x_{\text{univ}}}^{\text{cen}} k_z^{\text{univ}} \left. S_{y_{\text{univ}}}^{\text{cen}} \right|_b}{\omega\mu_{\text{cen}}}$$

$$M^{u\&\ell}_{9,5} = \kappa_x \frac{k_{\text{cen}}^2 - \left(k_{x_{\text{univ}}}^{\text{cen}}\right)^2}{j\omega\mu_{\text{cen}}\varepsilon_{\text{cen}}} \left. C_{y_{\text{univ}}}^{\text{cen}} \right|_b$$

$$M^{u\&\ell}_{9,6} = -\kappa_x \frac{k_{\text{cen}}^2 - \left(k_{x_{\text{univ}}}^{\text{cen}}\right)^2}{j\omega\mu_{\text{cen}}\varepsilon_{\text{cen}}} \left. S_{y_{\text{univ}}}^{\text{cen}} \right|_b$$

$$M^{u\&\ell}_{9,11} = \frac{jk_z^{\text{univ}} \sin\left(k_{y_{\text{TE}}}^{\text{low}} c\right)}{\varepsilon_{\text{low}}}$$

$$M^{u\&\ell}_{10,7} = -\kappa_x \frac{k_{\text{cen}}^2 - \left(k_{x_{\text{univ}}}^{\text{cen}}\right)^2}{j\omega\mu_{\text{cen}}\varepsilon_{\text{cen}}} \left. C_{y_{\text{univ}}}^{\text{cen}} \right|_b$$

$$M^{u\&\ell}_{10,8} = \kappa_x \frac{k_{\text{cen}}^2 - \left(k_{x_{\text{univ}}}^{\text{cen}}\right)^2}{j\omega\mu_{\text{cen}}\varepsilon_{\text{cen}}} \left. S_{y_{\text{univ}}}^{\text{cen}} \right|_b$$

$$M^{u\&\ell}_{10,12} = \frac{k_z^{\text{univ}} \sin\left(k_{y_{\text{TE}}}^{\text{low}} c\right)}{j\varepsilon_{\text{low}}}$$

$$M^{u\&\ell}_{11,3} = -\frac{k_{x_{\text{univ}}}^{\text{cen}} k_z^{\text{univ}} \left. C_{y_{\text{univ}}}^{\text{cen}} \right|_b}{\omega\mu_{\text{cen}}\varepsilon_{\text{cen}}}$$

$$M^{u\&\ell}_{11,4} = \frac{k^{\rm cen}_{x_{\rm univ}} k^{\rm univ}_z \left. S^{\rm cen}_{y_{\rm univ}}\right|_b}{\omega\mu_{\rm cen}\varepsilon_{\rm cen}}$$
$$M^{u\&\ell}_{11,5} = -\frac{k^{\rm cen}_{y_{\rm univ}} \left. S^{\rm cen}_{y_{\rm univ}}\right|_b}{\mu_{\rm cen}}$$
$$M^{u\&\ell}_{11,6} = -\frac{k^{\rm cen}_{y_{\rm univ}} \left. C^{\rm cen}_{y_{\rm univ}}\right|_b}{\mu_{\rm cen}}$$
$$M^{u\&\ell}_{11,11} = \frac{k^{\rm low}_{y_{\rm TE}} k^{\rm univ}_z \cos\left(k^{\rm low}_{y_{\rm TE}} c\right)}{\omega\mu_{\rm low}\varepsilon_{\rm low}}$$
$$M^{u\&\ell}_{12,1} = -\frac{k^{\rm cen}_{x_{\rm univ}} k^{\rm univ}_z \left. C^{\rm cen}_{y_{\rm univ}}\right|_b}{\omega\mu_{\rm cen}\varepsilon_{\rm cen}}$$
$$M^{u\&\ell}_{12,2} = \frac{k^{\rm cen}_{x_{\rm univ}} k^{\rm univ}_z \left. S^{\rm cen}_{y_{\rm univ}}\right|_b}{\omega\mu_{\rm cen}\varepsilon_{\rm cen}}$$
$$M^{u\&\ell}_{12,7} = \frac{k^{\rm cen}_{y_{\rm univ}} \left. S^{\rm cen}_{y_{\rm univ}}\right|_b}{\mu_{\rm cen}}$$
$$M^{u\&\ell}_{12,8} = \frac{k^{\rm cen}_{y_{\rm univ}} \left. C^{\rm cen}_{y_{\rm univ}}\right|_b}{\mu_{\rm cen}}$$
$$M^{u\&\ell}_{12,12} = -\frac{k^{\rm low}_{y_{\rm TE}} k^{\rm univ}_z \cos\left(k^{\rm low}_{y_{\rm TE}} c\right)}{\omega\mu_{\rm low}\varepsilon_{\rm low}}.$$

Appendix B
Constituents of Gauss Elimination

The constituents of the Gauss elimination performed on (13a) for use in Appendix C to obtain the matrix determinants are given as follows:

$$P_{5,i} = M^{\ell\&r}_{5,i} - \left(M^{\ell\&r}_{5,9} M^{\ell\&r}_{3,i} / M^{\ell\&r}_{3,9}\right), \quad \text{for } i = 1,3,6,8$$
$$P_{6,i} = M^{\ell\&r}_{6,i} - \left(M^{\ell\&r}_{6,10} M^{\ell\&r}_{4,i} / M^{\ell\&r}_{4,10}\right), \quad \text{for } i = 2,4,5,7$$
$$Q_{6,i} = M^{\ell\&r}_{11,i} - \left(M^{\ell\&r}_{11,11} M^{\ell\&r}_{9,i} / M^{\ell\&r}_{9,11}\right), \quad \text{for } i = 1,3,6,8$$
$$Q_{8,i} = M^{\ell\&r}_{12,i} - \left(M^{\ell\&r}_{12,12} M^{\ell\&r}_{10,i} / M^{\ell\&r}_{10,12}\right), \quad \text{for } i = 2,4,5,7$$
$$P_{7,i} = Q_{6,i} - (Q_{6,1}P_{5,i}/P_{5,1}), \quad \text{for } i = 3,6,8$$
$$Q_{10,i} = M^{\ell\&r}_{2,i} - \left(M^{\ell\&r}_{2,1} P_{5,i} / P_{5,1}\right), \quad \text{for } i = 3,6,8$$
$$Q_{12,i} = M^{\ell\&r}_{8,i} - \left(M^{\ell\&r}_{8,1} P_{5,i} / P_{5,1}\right), \quad \text{for } i = 3,6,8$$
$$P_{8,i} = Q_{8,i} - (Q_{8,2}P_{6,i}/P_{6,2}), \quad \text{for } i = 4,5,7$$
$$Q_{9,i} = M^{\ell\&r}_{1,i} - \left(M^{\ell\&r}_{1,2} P_{6,i} / P_{6,2}\right), \quad \text{for } i = 4,5,7$$
$$Q_{11,i} = M^{\ell\&r}_{7,i} - \left(M^{\ell\&r}_{7,2} P_{6,i} / P_{6,2}\right) \quad \text{for } i = 4,5,7$$
$$P_{10,i} = Q_{10,i} - (Q_{10,3}P_{7,i}/P_{7,3}), \quad \text{for } i = 6,8$$
$$Q'_{12,i} = Q_{12,i} - (Q_{12,3}P_{7,i}/P_{7,3}), \quad \text{for } i = 6,8$$
$$P_{9,i} = Q_{9,i} - (Q_{9,4}P_{8,i}/P_{8,4}), \quad \text{for } i = 5,7$$
$$Q'_{11,i} = Q_{11,i} - (Q_{11,4}P_{8,i}/P_{8,4}), \quad \text{for } i = 5,7$$
$$P_{11,7} = Q'_{11,7} - (Q'_{11,5}P_{9,7}/P_{9,5})$$
$$P_{12,8} = Q'_{12,8} - (Q'_{12,6}P_{10,8}/P_{10,6}).$$

Similarly, the constituents of the Gauss elimination conducted on (13b) are stated as follows:

$$U_{7,i} = M^{u\&\ell}_{5,i} - \left(M^{u\&\ell}_{5,9} M^{u\&\ell}_{3,i} / M^{u\&\ell}_{3,9}\right), \quad \text{for } i = 5 \text{ and } 6$$
$$U_{7,i} = M^{u\&\ell}_{5,i}, \quad \text{for } i = 3 \text{ and } 4$$
$$U_{5,i} = M^{u\&\ell}_{6,i} - \left(M^{u\&\ell}_{6,10} M^{u\&\ell}_{4,i} / M^{u\&\ell}_{4,10}\right), \quad \text{for } i = 7 \text{ and } 8$$
$$U_{5,i} = M^{u\&\ell}_{6,i}, \quad \text{for } i = 1 \text{ and } 2$$
$$V_{6,i} = M^{u\&\ell}_{11,i} - \left(M^{u\&\ell}_{11,11} M^{u\&\ell}_{9,i} / M^{u\&\ell}_{9,11}\right), \quad \text{for } i = 5 \text{ and } 6$$
$$V_{6,i} = M^{u\&\ell}_{11,i}, \quad \text{for } i = 3 \text{ and } 4$$
$$V_{8,i} = M^{u\&\ell}_{12,i} - \left(M^{u\&\ell}_{12,12} M^{u\&\ell}_{10,i} / M^{u\&\ell}_{10,12}\right), \quad \text{for } i = 7 \text{ and } 8$$
$$V_{8,i} = M^{u\&\ell}_{12,i}, \quad \text{for } i = 1 \text{ and } 2$$
$$U_{6,i} = V_{8,i} - (V_{8,1}U_{5,i}/U_{5,1}), \quad \text{for } i = 2,7,8$$
$$V_{9,i} = M^{u\&\ell}_{1,i} - \left(M^{u\&\ell}_{1,1} U_{5,i} / U_{5,1}\right), \quad \text{for } i = 2,7,8$$
$$V_{11,i} = M^{u\&\ell}_{7,i} - \left(M^{u\&\ell}_{7,1} U_{5,i} / U_{5,1}\right), \quad \text{for } i = 2,7,8$$
$$U_{11,i} = V_{9,i} - (V_{9,2}U_{6,i}/U_{6,2}), \quad \text{for } i = 7 \text{ and } 8$$
$$V'_{12,i} = V_{11,i} - (V_{11,2}U_{6,i}/U_{6,2}), \quad \text{for } i = 7 \text{ and } 8$$
$$U_{8,i} = V_{6,i} - (V_{6,3}U_{7,i}/U_{7,3}), \quad \text{for } i = 4,5,6$$
$$V_{10,i} = M^{u\&\ell}_{2,i} - \left(M^{u\&\ell}_{2,3} U_{7,i} / U_{7,3}\right), \quad \text{for } i = 4,5,6$$
$$V_{12,i} = M^{u\&\ell}_{8,i} - \left(M^{u\&\ell}_{8,3} U_{7,i} / U_{7,3}\right), \quad \text{for } i = 4,5,6$$
$$U_{9,i} = V_{10,i} - (V_{10,4}U_{8,i}/U_{8,4}), \quad \text{for } i = 5 \text{ and } 6$$
$$V'_{10,i} = V_{12,i} - (V_{12,4}U_{8,i}/U_{8,4}), \quad \text{for } i = 5 \text{ and } 6$$
$$U_{10,6} = V'_{10,6} - (V'_{10,5}U_{9,6}/U_{9,5})$$
$$U_{12,8} = V'_{12,8} - (V'_{12,7}U_{11,8}/U_{11,7}).$$

Appendix C
Matrix Determinants

It was mentioned in Section III.C that the matrix determinants may be obtained as the products of the diagonal elements in the row-echelon forms of the matrices. Doing so for both (13a) and (13b), the determinants of $[M^{\ell\&r}_{ij}]$ and $[M^{u\&\ell}_{ij}]$ are obtained as

$$\det\left[M^{\ell\&r}_{ij}\right] = M^{\ell\&r}_{3,9} M^{\ell\&r}_{4,10} M^{\ell\&r}_{9,11} M^{\ell\&r}_{10,12} \times P_{5,1}P_{6,2}P_{7,3}P_{8,4}P_{9,5}P_{10,6}P_{11,7}P_{12,8} \quad \text{(App-C1)}$$

$$\det\left[M^{u\&\ell}_{ij}\right] = M^{u\&\ell}_{3,9} M^{u\&\ell}_{4,10} M^{u\&\ell}_{9,11} M^{u\&\ell}_{10,12} \times M^{u\&\ell}_{6,1} U_{6,2} M^{u\&\ell}_{5,3} U_{8,4}U_{9,5}U_{10,6}U_{11,7}U_{12,8} \quad \text{(App-C2)}$$

in which the various terms have been provided in Appendices A and B.

REFERENCES

[1] H. C. Minnet and B. MacA. Thomas, "A method of synthesizing radiation patterns with axial symmetry," *IEEE Trans. Antennas Propag.*, vol. AP-14, no. 5, pp. 654–656, Sep. 1966.

[2] P. J. B. Clarricoats, "Theoretical analysis of cylindrical hybrid modes in a corrugated horn," *Electron. Lett.*, vol. 5, p. 187, May 1969.

[3] P. J. B. Clarricoats and P. K. Saha, "Propagation and radiation behaviour of corrugated feeds; Part 1—Corrugated-waveguide feed," *Proc. IEE*, vol. 118, no. 9, pt. H, pp. 1167–1176, Sep. 1971.

[4] P.-S. Kildal and E. Lier, "Hard horns improve cluster feeds of satellite antennas," *Electron. Lett.*, vol. 24, no. 8, pp. 491–492, Apr. 1988.

[5] M. Ng Mou Kehn and P.-S. Kildal, "Miniaturized rectangular hard waveguides for use in multi-frequency phased arrays," *IEEE Trans. Antennas Propag.*, vol. AP 53, no. 1, pp. 100–109, Jan. 2005.

[6] M. Abdelmoneium Ali, S. C. Ortiz, T. Ivanov, and A. Mortazawi, "Analysis and measurement of hard-horn feeds for the excitation of quasi-optical amplifiers," *IEEE Trans. Microw. Theory Techn.*, vol. 47, no. 4, pp. 479–487, Apr. 1999.

[7] S. F. Mahmoud, "Mode conversion on profiled corrugated conical horns," *Proc. IEE–Microw. Opt. Antennas*, vol. 130, no. 6, pt. H, pp. 415–419, 1983.

[8] L. C. Da Silva and M. G. C. Branco, "Analysis of the junction between smooth and corrugated cylindrical waveguides in mode converters," *IEEE Trans. Microw. Theory Techn.*, vol. 38, no. 6, pp. 800–802, Jun. 1990.

[9] A. J. Viitanen and T. M. Uusiputa, "Fields in anisotropic hard surface waveguide with application to polarisation transformer," *Proc. IEE–Microw., Antennas, Propag.*, vol. 148, no. 5, pp. 313–317, Oct. 2001.

[10] J. T. Bernhard and W. T. Joines, "Dielectric slab-loaded resonant cavity for applications requiring enhanced field uniformity," *IEEE Trans. Microw. Theory Techn.*, vol. 44, no. 3, pp. 457–460, Mar. 1996.

[11] J. Esteban and J. M. Rebollar, "Characterization of corrugated waveguides by modal analysis," *IEEE Trans. Microw. Theory Techn.*, vol. 39, no. 6, pp. 937–943, Jun. 1991.

[12] E. Garcia, J. A. Murphy, E. de Lera, and D. Segovia, "Analysis of the left-handed corrugated circular waveguide," *IET Microw. Antennas Propag.*, vol. 2, no. 7, pp. 659–667, 2008.

[13] E. Kowalski, D. S. Tax, M. A. Shapiro, J. R. Sirigiri, R. J. Temkin, T. S. Bigelow, and D. A. Rasmussen, "Linearly polarized modes of a corrugated metallic waveguide," *IEEE Trans. Microw. Theory Techn.*, vol. 58, no. 11, pp. 2772–2780, Nov. 2010.

[14] M. S. Narasimhan and K. R. Govind, "Radiation characteristics of a corrugated circular cylindrical waveguide horn excited in the TE_{11} mode," *IEEE Trans. Antennas Propag.*, vol. AP-36, no. 8, pp. 1147–1152, Aug. 1988.

[15] I. V. Lindell and A. H. Sihvola, "Dielectrically loaded corrugated waveguide: Variational analysis of a nonstandard eigenproblem," *IEEE Trans. Microw. Theory Techn.*, vol. MTT-31, no. 7, pp. 520–526, Jul. 1983.

[16] S. L. G. Lundqvist, "Electromagnetic waves in a cylindrical waveguide with infinite or semi-infinite wall corrugations," *IEEE Trans. Microw. Theory Techn.*, vol. 36, no. 1, pp. 28–33, Jan. 1988.

[17] I. G. Tigelis, M. Pedrozzi, P. G. Cottis, and J. L. Vomvoridis, "Calculation of eigenmodes in a nonperiodic corrugated waveguide," *IEEE Trans. Microw. Theory Techn.*, vol. 45, no. 2, pp. 236–344, Feb. 1997.

[18] Y. Takeichi, T. Hashimoto, and F. Takeda, "The ring-loaded corrugated waveguide," *IEEE Trans. Microw. Theory Techn.*, vol. MTT-19, no. 12, pp. 947–950, Dec. 1971.

[19] A. M. B. Al-Hariri, A. D. Olver, and P. J. B. Clarricoats, "Low-attenuation properties of corrugated rectangular waveguide," *Electron. Lett.*, vol. 15, no. 15, pp. 304–305, Jul. 1974.

[20] L. W. Epp, D. J. Hoppe, and D. T. Kelley, "A TE/TM modal solution for rectangular hard waveguides," *IEEE Trans. Microw. Theory Techn.*, vol. 54, no. 3, pp. 1048–1054, Mar. 2006.

[21] I. A. Eshrah, A. A. Kishk, A. B. Yakovlev, and A. W. Glisson, "Spectral analysis of left-handed rectangular waveguides with dielectric-filled corrugations," *IEEE Trans. Antennas Propag.*, vol. AP-53, no. 11, pp. 3673–3683, Nov. 2005.

[22] M. Mineo and C. Paoloni, "Corrugated rectangular waveguide tunable backward wave oscillator for terahertz applications," *IEEE Trans. Electron Devices*, vol. 57, no. 6, pp. 1481–1484, Jun. 2010.

[23] R. Pierre, G. Tayeb, B. Gralak, and S. Enoch, "Quasi-TEM modes in rectangular waveguides: A study based on the properties of PMC and hard surfaces," *J. Modern Opt.*, vol. 56, no. 4, pp. 530–538, 2009.

[24] M. Ng Mou Kehn, "Rapid surface-wave dispersion and plane-wave reflection analyses of planar corrugated surfaces by asymptotic corrugations boundary conditions even for oblique azimuth planes," *IEEE Trans. Antennas Propag.*, vol. 61, no. 5, pp. 2695–2707, May 2013.

[25] C. A. Balanis, *Advanced Engineering Electromagnetics*. New York, NY, USA: Wiley, 1989.

Malcolm Ng Mou Kehn (S'02–M'06–SM'13) was born in Singapore, on September 26, 1976. He received the B.Eng. (honors) degree from the National University of Singapore, Singapore, in 2001, and the Licentiate and Ph.D. degrees from the Chalmers University of Technology, Göteborg, Sweden, in and 2005, respectively, all in electrical engineering.

From 2006 to 2008, he was a Postdoctoral Fellow with the Department of Electrical and Computer Engineering, University of Manitoba, Winnipeg, MB, Canada. He then joined Concordia University, Montreal, QC, Canada, for one year. In August 2009, he joined the Department of Electrical Engineering, National Chiao Tung University (NCTU), Hsinchu, Taiwan, initially as an Assistant Professor, and since August 2012, as an Associate Professor. From 2002 and 2006, he was actively involved in research projects funded by the Swedish Defense Research Agency. During Autumn 2004, he spent several months with the University of Siena, Siena, Italy, for a research visit. In December 2004, he visited the University of Zagreb, Zagreb, Croatia, as an Invited Speaker where he gave an IEEE lecture in connection with IEEE Croatia Chapter activities. From 2006 to 2009, he was extensively involved in numerous projects supported by Canadian industry and national research bodies. Since August 2009, he has been securing research project grants funded by the National Science Council of Taiwan.

Dr. Ng Mou Kehn was the recipient of the Union Radio-Scientifique Internationale (URSI) Young Scientist Award in 2007 and the NCTU Meritorious Teaching Award in 2013.